Agricultural and Forest Meteorology 340 (2023) 109600

Contents lists available at ScienceDirect

Agricultural and Forest Meteorology

journal homepage: www.elsevier.com/locate/agrformet

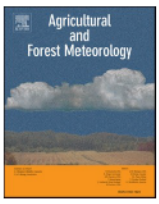

Snow-corrected vegetation indices for improved gross primary productivity assessment in North American evergreen forests

Ran Wang [a,*], David R. Bowling [b], John A. Gamon [a], Kenneth R. Smith [b], Rong Yu [c,d], Gabriel Hmimina [e], Masahito Ueyama [f], Asko Noormets [g], Thomas E. Kolb [h], Andrew D. Richardson [i,j], Charles P.A. Bourque [k], Rosvel Bracho [l], Peter D. Blanken [m], T. Andrew Black [n], M. Altaf Arain [o]

[a] School of Natural Resources, University of Nebraska-Lincoln, Lincoln, NE 68583, USA
[b] School of Biological Sciences, University of Utah, Salt Lake City, UT 84112, USA
[c] State Key Laboratory of Subtropical Silviculture, Zhejiang A&F University, Hangzhou, China
[d] Key Laboratory of Carbon Cycling in Forest Ecosystems and Carbon Sequestration of Zhejiang Province, Zhejiang A&F University, Hangzhou, China
[e] Laboratoire de Météorologie Dynamique, IPSL, CNRS/UPMC, Paris 75005, France
[f] Graduate School of Agriculture, Osaka Metropolitan University, Sakai, Osaka 599-8531, Japan
[g] Department of Ecosystem Science and Management, Texas A&M University, College Station, TX 77843, USA
[h] School of Forestry, Northern Arizona University, Flagstaff, AZ 86011, USA
[i] School of Informatics, Computing and Cyber Systems, Northern Arizona University, Flagstaff, AZ 86011, USA
[j] Center for Ecosystem Science and Society, Northern Arizona University, Flagstaff, AZ 86011, USA
[k] Faculty of Forestry and Environmental Management, University of New Brunswick, Fredericton, NB E3B 5A3, Canada
[l] School of Forest, Fisheries and Geomatics Sciences. University of Florida, Gainesville, FL 32611, USA
[m] Department of Geography, University of Colorado Boulder, Boulder, CO 80302, USA
[n] Faculty of Land and Food Systems, University of British Columbia, Vancouver, BC V6T 1Z4, Canada
[o] School of Earth, Environment and Society and McMaster Centre for Climate Change, McMaster University, Hamilton, ON L8S 4K1, Canada

ARTICLE INFO

Keywords:
Evergreen
GPP
MODIS
Chlorophyll-carotenoid index (CCI)
NIRv
Snow

ABSTRACT

North American evergreen forests cover large areas and influence the global carbon cycle. Satellite remote sensing has been used to track the phenology of ecosystem photosynthesis of these forests by detecting variation in vegetation optical properties associated with physiological and structural features, and most of these methods have been closely tied to vegetation greenness. However, in evergreens, the application of satellite data to monitor photosynthetic phenology is often limited by the lack of sensitivity of greenness-based indices. In this study, we identified 47 evergreen forest flux sites in North America that had MODIS observation overlapping with the flux tower records. We then calculated four vegetation indices using MODIS MAIAC data (MCD19A1), including NDVI, CCI, NIRv, and kNDVI, for the 47 flux sites and evaluated relationships between gross primary productivity (GPP) and vegetation indices across the North American evergreen forests. Our results showed that snow had substantial effects on the performance of all vegetation indices in tracking GPP phenology, particularly in the early spring when rapid changes occurred to both GPP and snow cover. Different vegetation indices were affected differently, indicating contradictory and confounding effects of snow on these indices. After correcting for the snow effects, both CCI and NIRv performed well in tracking GPP phenology, albeit for different reasons. CCI is sensitive to seasonal changes in the relative levels of chlorophyll and carotenoid pigments, which are closely tied to GPP phenology in evergreens. NIRv is sensitive to the absorbed photosynthetically active radiation and to the contribution of deciduous components to the overall optical properties. We also found that correlations between GPP and vegetation indices varied among ecoregions and climate classes. In general, regions with pronounced seasonal GPP patterns had stronger correlations between GPP and greenness-based indices than regions with weaker seasonal GPP patterns. These biome differences were less pronounced for CCI. The snow

* Corresponding author.
E-mail address: ranwangrs@gmail.com (R. Wang).

https://doi.org/10.1016/j.agrformet.2023.109600
Received 1 December 2022; Received in revised form 20 May 2023; Accepted 8 July 2023

artifacts and complementary vegetation index effects reported here should be considered in any large-scale studies of GPP using reflectance-based indices from optical satellites.

1. Introduction

Evergreen forest ecosystems occupy approximately 21.6 million km^2 area representing ~49.3% of global tree cover (FAO and UNEP, 2020). In North America, evergreen forests cover large expanses, including the boreal (taiga) forests in the northern high latitude, coastal forests of the Pacific Northwest, eastern coastal forests along the Appalachians, forests of the Rocky Mountains, and other western montane forests. These evergreen forests provide crucial ecosystem goods and services, including flood regulation, water purification, timber, and wildlife habitat (Hassan et al. 2005; Wells et al., 2020), and play important roles in regulating global climate and global carbon cycle in part due to their geographic extent (Bonan, 2008). The distribution and growth of evergreen forests are influenced by climate, particularly temperature and precipitation, but these effects vary among ecoregions (Bowling et al., 2018; Ensminger et al., 2004; Sevanto et al., 2006; Turcotte et al., 2009). In recent years, extensive warming and drying, coupled with insect infestations, fires and harvests, have led to evergreen forest decline in much of North America, from the southwest to the boreal regions of Canada and Alaska (Kirilenko and Sedjo, 2007; Williams et al., 2013; McDowell et al., 2016; White et al., 2017; Stralberg et al., 2020; Wells et al., 2020). These recent trends suggest that a warmer climate might not necessarily lead to higher productivity of evergreen forests especially in regions concurrently experiencing a decrease in precipitation (Ammer, 2019; Zhang et al., 2022). Long-term changes in climate can also have a lasting effect on ecosystem productivity by causing a shift in species composition and thereby altering community productivity potential (Dial et al., 2022; Thompson et al., 2013).

Satellite remote sensing can provide repeated, standardized measurements over large areas and can serve as a tool to estimate ecosystem gross primary productivity (GPP) at different scales. The widely used Normalized Difference Vegetation Index (NDVI) (Running et al., 2004) and newly developed products that are based on red and near-infrared (NIR) bands, including NIRv (Badgley et al., 2017) and kNDVI (Camps-Valls et al., 2021), have been used to monitor GPP phenology seasonal pattern of GPP including timing and magnitude of different ecosystems, often at large spatial and temporal scales (e.g. 1 km pixel size and monthly timesteps). Studies employing these remotely sensed indices using empirical functions or the light use efficiency model have generally revealed site- and biome-based differences in the fidelity of their relationships with GPP (Heinsch et al., 2003; Running et al., 2004; Badgley et al., 2017; Ryu et al., 2019). Compared to deciduous forests, predicting GPP phenology based on NDVI remains challenging for evergreen forests due to the limited seasonal variation in green canopy structure (Gamon et al., al.,1995; Running et al., 2004; Hmimina et al., 2013; Peng et al., 2017). NDVI-based indices track changes in greenness based on changes in chlorophyll, canopy growth or senescence (Zeng et al., 2022), but miss the subtle changes in photosynthetic activity caused by physiological regulation, which often is the preponderant influence on GPP phenology in evergreens (Gamon et al., 2015&2016, 2015; Springer et al., 2017; Wong et al., 2020). In a previous study that compared GPP and NDVI-based vegetation indices derived using MODIS data, the lowest correlations between GPP and VIs were found for evergreen forests among all vegetated biomes examined (Camps-Valls et al., 2021). In contrast, indices based on the photoprotective roles of carotenoid pigments, e.g., the Photochemical Reflectance Index (PRI) and the Chlorophyll-Carotenoid Index (CCI), have shown good fidelity to GPP phenology in evergreens (Gamon et al., 2016; Wong et al., 2022). These results indicate complementary behavior of vegetation indices (the complementarity hypothesis; Gamon 2015, Gamon et al., 2016), with some addressing GPP phenology via greenness and others detecting less visible photoregulatory processes associated with carotenoid pigments and non-photochemical quenching of fluorescence.

CCI was designed to monitor GPP phenology of evergreen forests because of its sensitivity to seasonal pigment change, particularly the relative levels of chlorophyll and carotenoid pigments (Gamon et al., 2016). Sometimes called MODIS PRI (Rahman et al., 2004; Drolet et al., 2008; Middleton et al., 2016), the CCI formula is slightly different from the original PRI formula, which was originally designed to monitor the diurnal activity of the xanthophyll cycle (Gamon et al., 2016). Like PRI, CCI is sensitive to seasonally changing pigment pools, but unlike PRI, it is available from the MODIS sensors (Aqua and Terra), making it readily available for global analyses of GPP phenology. The long-term variation of the ratio between chlorophyll and carotenoid pigments detected by CCI indicates changes in vegetation photosynthetic activity (Wong and Gamon, 2015; Gamon et al., 2016; Bowling et al., 2018; Cheng et al., 2020; Wong et al., 2020; Walter-McNeill et al., 2021). For example, increased carotenoids in the winter period reflect more photoprotection for overwintering evergreen species (Demmig-Adams and Adams, 1996; Verhoeven, 2014; Bowling et al., 2018). Several studies have shown that CCI can track GPP phenology in both evergreen and deciduous trees at different spatial scales (Gamon et al., 2016; Springer et al., 2017; Wong et al., 2020; Pierrat et al., 2022; Yang et al., 2022); however, like all reflectance-based vegetation indices, CCI is also affected by snow cover, which can perturb its relationship with GPP. While these snow-cover effects have been considered before for some indices (e.g., NDVI; Myers-Smith et al., 2020), they have not been well studied for others (e.g., CCI). The overall influence of snow on remote observations of GPP phenology is unclear, as most studies have not attempted to correct for the effects of snow, leaving open the possibility of significant artifacts in our interpretation of GPP.

Snow typically has very high visible reflectance and very low shortwave-infrared reflectance (Dozier et al., 2009) and therefore affects all reflectance-based vegetation indices to some degree. Snow coverage can be readily estimated using the MODIS Normalized Difference Snow Index (NDSI) that utilizes the green (B4) and SWIR (B6) bands (Riggs et al., 2016). However, NDSI may fail to detect snow pixels due to the malfunction of a large part of Aqua band 6 detectors (Gladkova et al., 2012). Snow detection using NDSI is also sensitive to conditions with low visible reflectance, for example, low illumination when solar zenith angle is 70 and the landscape shadowed by clouds or terrain (Lv and Pomeroy, 2019) and forest coverage (Xin et al. 2012; Wang et al., 2018). As a consequence, correcting for snow cover can be complicated, yet remains critical because snow-affected satellite-based vegetation indices can confound the relationship between GPP and vegetation indices, particularly in northern latitude and high-altitude regions (Jin and Eklundh, 2014; Jin et al., 2017; Springer et al., 2017). Thus, it is likely that changes in apparent GPP based on vegetation indices are influenced by snow cover, causing uncertainty in satellite-derived estimates of seasonal and interannual GPP patterns and trends (Myers-Smith et al., 2020).

In this study, we integrated surface flux tower eddy covariance flux data with MODIS vegetation indices across different types of evergreen forests in North America, ranging from subtropical to subarctic climates, to test the feasibility of different MODIS-derived vegetation indices to track GPP in evergreen forests. Our major hypotheses were: (1) snow cover has a substantial effect on the performance of vegetation indices in tracking GPP phenology, and removing snow-based artifacts improves the relationship between GPP and vegetation indices; (2) CCI performs better than NDVI-based indices in monitoring GPP of evergreen forests because of its sensitivity to seasonal pigment change; and (3) the relationships between GPP and VIs vary geographically (e.g., by

ecoregion) due to contrasting climate controls and forest composition on the physiological function and optical properties of evergreen forests.

2. Methods

2.1. Flux sites

Using three eddy covariance databases including FLUXNET2015 (Pastorello et al., 2020), AmeriFlux, and the National Ecological Observatory Network (NEON), we identified evergreen-dominated eddy covariance flux tower sites in North America that had MODIS observation overlapping with flux tower observations (n = 99 towers). We applied a quality check procedure to the flux data and shortened the list of sites by: (1) omitting sites that had less than one year of data; (2) omitting sites with failed net ecosystem exchange (NEE) partitioning algorithms and failed GPP analysis (details below); and (3) omitting sites located in topographically complex terrain, as described below. We used the MERIT global digital elevation model (Yamazaki et al., 2017) and Landsat NDVI to evaluate the landscape within the flux footprints in both vertical and horizontal dimensions. The spatial resolutions of MERIT DEM and Landsat NDVI are 3 arc seconds (~90 m at the equator) and 30 m, respectively. We calculated the standard deviation of elevation and summer NDVI during the flux sampling time periods within 1 km^2 areas at each flux site and eliminated sites in mountainous areas (standard deviation of elevation > 50 m) and heterogenous vegetation cover types (standard deviation of NDVI > 0.2). This site suitability analysis was done using Google Earth Engine (Gorelick et al., 2017). This procedure led to a final selection of 47 evergreen flux tower sites for our analysis, spanning 6 ecoregions and 6 climate classes (Fig. 1, Table 1).

2.2. Flux tower data processing

Flux data from these 47 sites were processed using the REddyProc package in R (Wutzler et al., 2018). We used two methods, including daytime (Lasslop et al., 2010) and nighttime (Reichstein et al., 2005) to partition the eddy covariance measured NEE into GPP based on the calculated ecosystem respiration for each site, with air temperature as the temperature driver, and a 50% friction velocity threshold. The daily GPP derived from the daytime partitioning method (Lasslop et al., 2010) is presented in the main text, while that from the nighttime partitioning is presented in the supplemental materials.

2.3. MODIS MAIAC data

MODIS Collection 6 data were corrected to surface reflectance using the Multi-Angle Implementation of Atmospheric Correction algorithm (MAIAC; Lyapustin et al., 2018, 2012). The MAIAC product (i.e., MCD19A1) offers land surface bidirectional reflectance factor for both MODIS land and ocean bands (bands 1–12) at 1 km spatial resolution on a per-observation basis in daily files. The high temporal resolution of the MAIAC product potentially provides more information on vegetation phenology than the 16-day composite MODIS data (Hmimina et al., 2013; Wang et al., 2020). To keep a large dataset for snow detection (details below), we did not filter data with large view zenith angles (Middleton et al., 2016) or solar zenith angles. Using a threshold of 45° view zenith angle can remove more than 40% of the data (Wang et al., 2020), and winter observations for high latitude regions often have large solar zenith angles. To generate a daily product for vegetation indices, we used the observation with minimum view zenith angle when multiple data points were available within a single day.

We explored the relationship between flux GPP and four MODIS vegetation indices (VIs) including NDVI Running et al., 2004), CCI (Gamon et al., 2016), NIRv (Badgley et al., 2017), and kNDVI (Camps-Valls et al., 2021) that have been used to track GPP phenology across different ecosystems. For each site, we used the pixel that had the minimum distance between the center of pixel and the flux site. The MODIS VIs were calculated from MODIS band ("B") numbers indicated by the subscripts in Eqs. (1)–(3) below. In Eq. (4), "tanh" stands for the hyperbolic tangent function (Camps-Valls et al., 2021).

$$NDVI = \frac{B_2 - B_1}{B_2 + B_1} \quad (1)$$

$$NIRv = (NDVI - 0.08) \times B_2 \quad (2)$$

$$CCI = \frac{B_{11} - B_1}{B_{11} + B_1} \quad (3)$$

$$kNDVI = \tanh\left(NDVI^2\right) \quad (4)$$

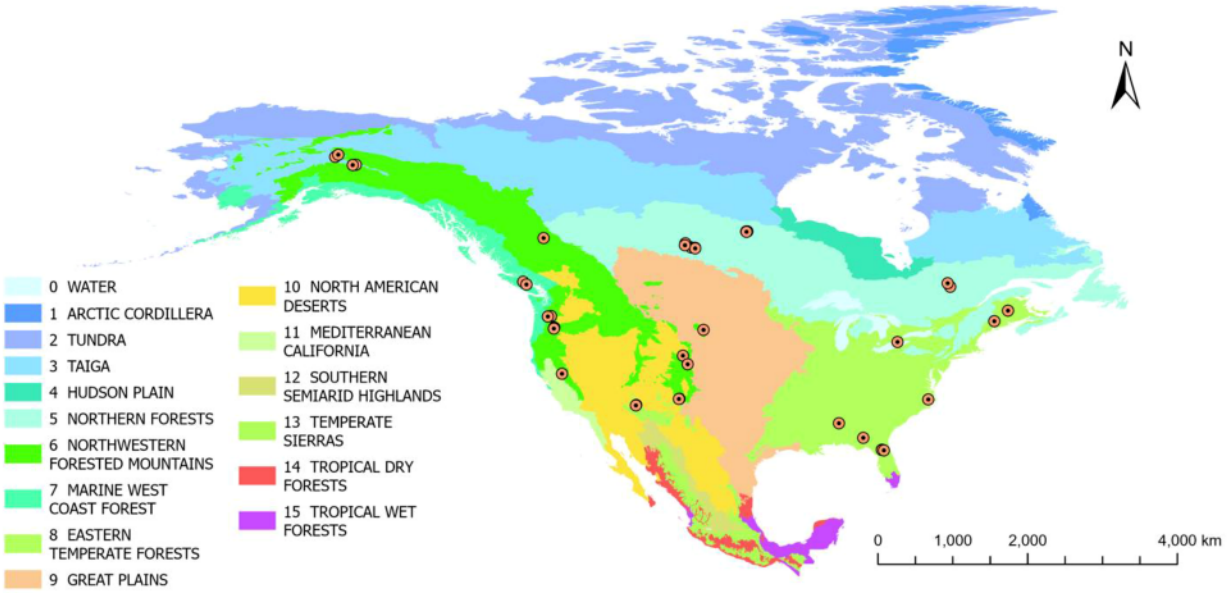

Fig. 1. Locations of evergreen forest flux towers and related ecoregions. Level-1 ecoregion map of North America was obtained from the United States Environmental Protection Agency (McMahon et al., 2001; Omernik and Griffith, 2014).

Table 1
Locations, climates and ecoregions of flux sites used in this study. Flux sites are sorted by latitude (from North to South). MAP and MAT indicate mean annual precipitation and mean annual temperature, respectively.

Site ID	Latitude ( )	Longitude ( )	Elevation (m)	MAP (mm)	MAT (C)	Level-1 Ecoregion	Koppen Climate Class	Refs.
US-Prr	65.12	147.49	210	275	2.00	Taiga	Subarctic	Iwahana et al. (2019)
US-Uaf	64.87	147.86	155	263	2.90	Taiga	Subarctic	Ueyama et al. (2023)
US-Bn1	63.92	145.38	518	289	0.29	Northwestern forested mountains	Dry continental	Randerson (2016)
US-xDJ	63.88	145.75	529	300	2.00	Northwestern forested mountains	Subarctic	NEON (2022)
CA-NS3	55.91	98.38	260	502	2.87	Northern forests	Subarctic	Goulden (2019)
CA-NS2	55.91	98.52	260	499	2.88	Northern forests	Subarctic	Goulden (2019)
CA-Man	55.88	98.48	259	520	3.20	Northern forests	Subarctic	Amiro (2016)
CA-NS1	55.88	98.48	260	500	2.89	Northern forests	Subarctic	Goulden (2019)
CA-NS5	55.86	98.49	260	500	2.86	Northern forests	Subarctic	Goulden (2019)
CA-LP1	55.11	122.84	751	570	2.00	Northwestern forested mountains	Mediterranean (Csa)	Black (2022)
CA-SF1	54.49	105.82	536	470	0.40	Northern forests	Subarctic	Amiro (2020)
CA-SF2	54.25	105.88	520	470	0.40	Northern forests	Subarctic	Amiro (2019)
CA-Obs	53.99	105.12	629	405	0.79	Northern forests	Subarctic	Black (2016)
CA-SJ2	53.95	104.65	580	430	0.11	Northern forests	Subarctic	Barr and Black (2018)
CA-Ojp	53.92	104.69	579	430	0.12	Northern forests	Subarctic	Black (2019)
CA-SJ1	53.91	104.66	580	430	0.13	Northern forests	Subarctic	Barr (2018)
CA-SJ3	53.88	104.65	498	433	0.13	Northern forests	Subarctic	Barr (2018)
CA-Ca2	49.87	125.29	300	1474	9.86	Marine west coast forest	Marine west coast	Black (2018)
CA-Qfo	49.69	74.34	382	962	0.36	Northern forests	Subarctic	Margolis (2019)
CA-Ca3	49.53	124.90	162	1676	9.94	Marine west coast forest	Marine west coast	Black (2023)
CA-Qcu	49.27	74.04	392	949	0.13	Northern forests	Subarctic	Margolis (2016)
CA-Na1	46.47	67.10	341	1102	7.09	Eastern temperate forests	Warm summer continental	Bourque (2018)
US-Wrc	45.82	121.95	371	2452	8.80	Northwestern forested mountains	Mediterranean	Wharton (2016)
US-xWR	45.82	121.95	407	2225	9.20	Northwestern forested mountains	Mediterranean	NEON (2022)
US-xAB	45.76	122.33	363	2450	10.00	Marine west coast forest	Mediterranean	NEON (2022)
US-Ho2	45.21	68.75	91	1064	5.13	Eastern temperate forests	Warm summer continental	Hollinger (2021)
US-Ho1	45.20	68.74	60	1070	5.27	Eastern temperate forests	Warm summer continental	Hollinger (2021)
US-Me2	44.45	121.56	1253	523	6.28	Northwestern forested mountains	Mediterranean	Law (2022)
US-Me5	44.44	121.57	1188	590	6.47	Northwestern forested mountains	Mediterranean	Law (2021)
US-Me6	44.32	121.61	998	494	7.59	Northwestern forested mountains	Mediterranean	Law (2021)
US-Me3	44.32	121.61	1005	719	7.07	Northwestern forested mountains	Mediterranean	Law (2018)
US-Blk	44.16	103.65	1718	573	6.23	Northwestern forested mountains	Warm summer continental	Meyers (2016)
CA-TP4	42.71	80.36	184	1036	8.00	Eastern temperate forests	Warm summer continental	Arain (2018)
US-CPk	41.07	106.12	2750	545	6.10	Northwestern forested mountains	Subarctic	Ewers et al. (2016)
US-NR1	40.03	105.55	3050	800	1.50	Northwestern forested mountains	Subarctic	Blanken et al. (2022)
US-Blo	38.90	120.63	1315	1226	11.09	Northwestern forested mountains	Mediterranean	Goldstein (2019)
US-Vcm	35.89	106.53	3003	646	6.40	Northwestern forested mountains	Warm summer continental	Litvak (2022)
US-Vcp	35.86	106.60	2500	550	9.80	Northwestern forested mountains	Warm summer continental	Litvak (2022)
US-NC2	35.80	76.67	5	1320	16.60	Eastern temperate forests	Humid subtropical	Noormets et al. (2022)
US-Fmf	35.14	111.73	2160	546	9.50	Temperate sierras	Mediterranean	Dore and Kolb (2019)
US-Fuf	35.09	111.76	2180	562	8.70	Temperate sierras	Mediterranean	Dore and Kolb (2019)
US-xTA	32.95	87.39	135	1382	17.20	Eastern temperate forests	Humid subtropical	NEON (2022)
US-xJE	31.19	84.47	44	1307	19.20	Eastern temperate forests	Humid subtropical	NEON (2022)
US-SP2	29.76	82.25	50	1314	20.07	Eastern temperate forests	Humid subtropical	Bracho and Martin, 2016a
US-SP3	29.75	82.16	50	1312	20.25	Eastern temperate forests	Humid subtropical	Bracho and Martin, 2016b
US-SP1	29.74	82.22	50	1309	20.06	Eastern temperate forests	Humid subtropical	Bracho and Martin, 2016c
US-xSB	29.69	81.99	45	1302	20.90	Eastern temperate forests	Humid subtropical	NEON (2022)

2.4. Snow removal algorithm applied to MODIS VIs

To evaluate the snow effects on MODIS vegetation indices, we used data collected at the CA-Qfo flux site (located in Quebec, Canada, latitude: 49.69°, longitude: −74.34°), which is also registered as site Chibougamau within the PhenoCam network (Seyednasrollah et al., 2019). The overlapping observations of eddy covariance, MODIS, and PhenoCam imagery in 2009 at this black spruce and jack pine dominated forest site enabled us to delineate the confounding effects of snow on vegetation indices. The snow-affected periods, including spring snow melt, were visually identified from the PhenoCam images, which clearly revealed periods of snow cover for this particular site due to an area of bare ground included in the images.

To detect and then minimize the snow effects on the GPP-VI relationships, we developed a method to identify snow pixels by combining NDSI, CCI and kNDVI, because combining multiple indices leads to improved snow detection for forested areas over using NDSI alone (Lv and Pomeroy, 2019; Wang et al., 2018). In this study, we used CCI and kNDVI in snow detection. Unlike NDVI-based indices, snow increases CCI values (Figure S1 in the supplemental materials). kNDVI was designed to be insensitive to NDVI variation when NDVI is low (Camps-Valls et al., 2021). For evergreen forests, these low NDVI values are most likely caused by snow cover. Thus, kNDVI values are constantly low, with limited variations during snow-covered periods (Figure S1 in the supplemental materials). This combination of CCI and kNDVI is particularly useful to separate snow-affected data from snow free data in the kNDVI-CCI space, which has relatively low kNDVI values and high CCI values (Figure S2 in the supplemental materials). For sites that have a long snow-affected period (annual total number of snow-affected days > 30), we identified snow pixels based on NDSI and trained a binary support vector machine (SVM; Boser et al., 1992) to distinguish snow-affected pixels using data collected during the flux and MODIS data overlap for each site. To automate model selection for each site, we used Bayesian optimization in Matlab 2021b to optimize hyperparameters of each SVM classification model (Gelbart et al., 2014; Snoek et al., 2012). In each SVM snow detection model, we used NDSI to label pixels affected by snow and used CCI and kNDVI as inputs of SVM. We tested the SVM classification accuracy at each site using 10-fold cross-validation. We then applied the snow detection algorithm to all the data at this site to identify snow-affected data that might be missed by using NDSI alone (Figs. 2, S1 and S2 in the supplemental materials). We removed the data either labeled as snow according to NDSI or classified as snow by the binary SVM model. For sites whose total number of annual snow-affected days was less than 30 days, we removed the snow-affected pixels identified with NDSI, because a small training sample had the potential to decrease the accuracy of SVM classification. After removing snow-affected data, we then used asymmetric Gaussian functions (Jönsson and Eklundh, 2004) to fit the snow-free data and extend the fitted curve to estimate the theoretical snow-free vegetation index values in the winter. To quantify the effectiveness of snow removal algorithm, we calculated the Pearson correlation coefficients between daily GPP and vegetation indices before and after snow removal for the 47 sites.

2.5. Contributions of snow artifacts vs. biological effects to vegetation index variations

To evaluate the extent of snow influence for each index, we calculated a series of "delta" values due to snow, vegetation, and all factors combined. To do this, we compared the change in yearly VI values (i.e., the "total" range across the annual period in VI values; "yearly" delta VI) to the change due to snow artifacts (i.e., "snow-affected" delta VI values) and due to actual vegetation change (i.e., "snow-free" delta values, the

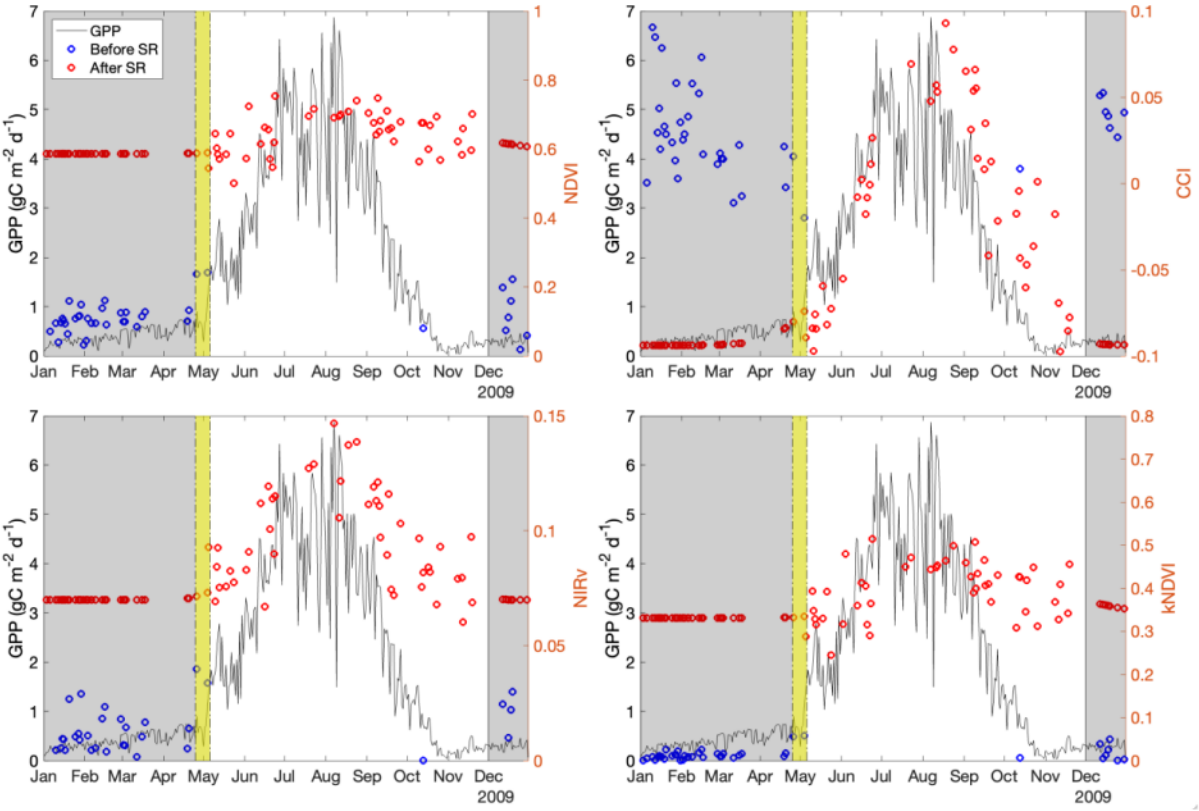

Fig. 2. Seasonal course of GPP (black lines) and vegetation indices (NDVI, CCI, NIRv, and kNDVI) before (blue points) and after (red points) snow removal ("SR"). Data were collected from the CA-Qfo flux site in 2009. Grey-shaded areas denote snow-affected periods, and the vertical yellow band indicates snow-melt period in the late spring based on visual inspection of PhenoCam imagery. We also identified an additional snow day on October 13, 2009 using PhenoCam imagery.

change in VI values due to the residual effect of vegetation, following correction for snow cover). Yearly deltas were calculated by subtracting the minimum value from the maximum value within a year. Snow-free ("vegetation") deltas were calculated by subtracting the minimum value from the maximum value from May – October. Snow-affected deltas were calculated by subtracting the minimum value from the maximum value in the snow affected months (November to April). This methodology allowed us to evaluate the annual change in a vegetation index due to actual biological effects associated with vegetation structural and physiological changes versus those due to snow artifacts.

2.6. Relationships between VIs and apar and ε in the LUE model

To explore the relationships between MODIS vegetation indices and different terms in the light use efficiency (LUE) model, we combined *APAR* using daily maximum *PPFD* from the flux measurements with MODIS *NDVI* to provide an indicator of *fAPAR*. Considering the overestimation of MODIS *fAPAR* especially for sparse forests in boreal region (Iwata et al., 2013; Yan et al., 2016), we directly estimated *fAPAR* by utilizing a linear relationship between NDVI and *fAPAR* (Sims et al., 2006). Then, the efficiency of utilizing light in photosynthesis (ε) was calculated as

$$\varepsilon = \frac{GPP}{APAR} = \frac{GPP}{PPFD \times fAPAR} = \frac{GPP}{PPFD \times f(NDVI)} \quad (5)$$

3. Results

3.1. Snow effects on MODIS VIs

The influence of snow cover varied with vegetation index at the CA-Qfo site (Figs. 2 and 3). All vegetation indices were affected by snow, which increased CCI values, but decreased NDVI-based indices (NDVI, NIRv, and kNDVI). Among the NDVI-based indices, kNDVI was least sensitive to changes in snow cover (exhibiting least variation) due to the compressed variation when NDVI values were low during snow-covered periods. The contrasting responses to snow cover of CCI and kNDVI to the presence of snow enabled snow detection with these two indices (Figs. 2, S1 and S2 in the supplemental materials).

The magnitude of changes in the vegetation indices due to snow vs. vegetation phenology became clear by means of "delta" values for each index, defined as the absolute difference between summer maxima to winter minima with and without snow correction (Fig. 3). All indices showed large snow effects, which we refer to as "snow artifacts" because they represent the potentially confounding effects of snow on relationships between GPP and vegetation indices. In all cases, the snow removal algorithm reduced the snow effects on vegetation indices (Figs. 2 and 3).

The performance of vegetation indices in tracking GPP phenology was clearly confounded by snow coverage. At the CA-Qfo site, snow cover greatly exaggerated the seasonal variation in NDVI; most of the seasonal variation in NDVI-based indices occurred during transitions in snow-cover when daily GPP was less than 1 g C m^{-2} d^{-1} (Figs. 3 and 4), revealing a clear artifact of snow cover on the GPP-NDVI relationship.

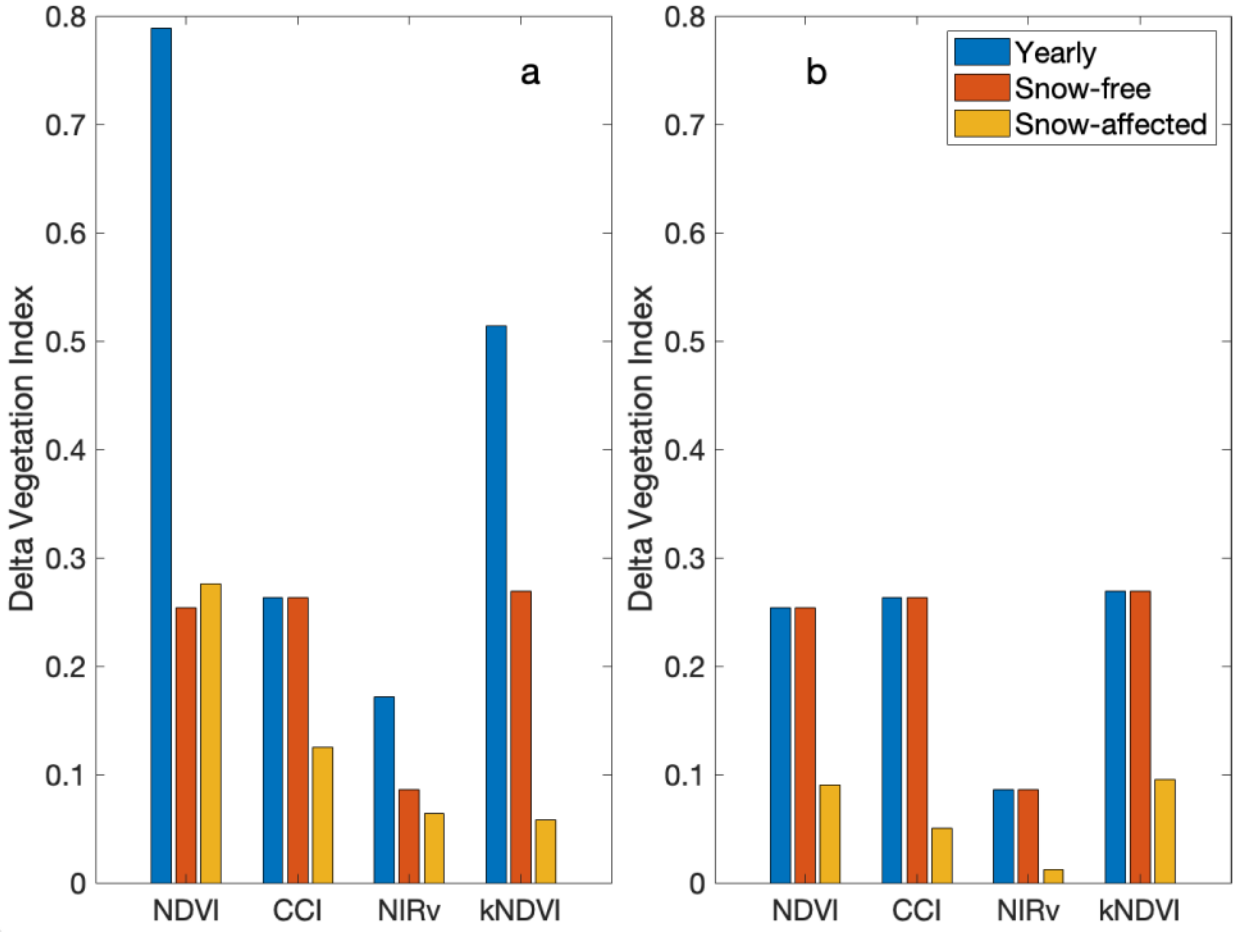

Fig. 3. Seasonal delta vegetation index (NDVI, CCI, NIRv, and kNDVI) values before (a) and after (b) snow removal in 2009. Yearly (blue) deltas were calculated by subtracting the minimum value from the maximum value within a year. Snow-free (red) deltas were calculated by subtracting the minimum value from the maximum value from May – October, and represent the delta VI values attributable to vegetation change. Snow-affected (yellow) deltas were calculated by subtracting the minimum value from the maximum value in the snow affected months (November to April). Data were collected from the CA-Qfo flux site.

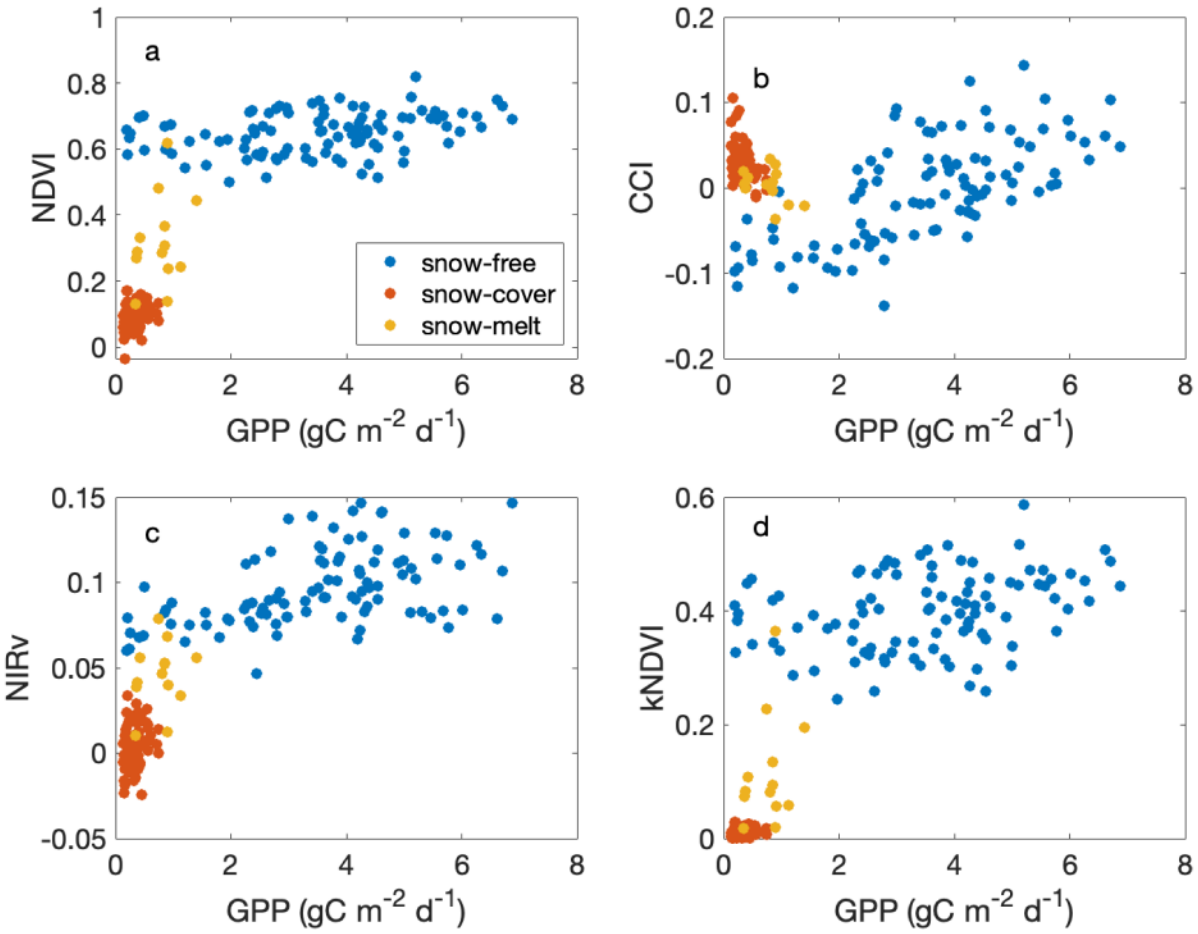

Fig. 4. Relationships between GPP and different vegetation indices for different seasonal periods, illustrating effects of snow-cover (red points) and snow-melt (orange points) on the correlation between GPP and vegetation indices. Data were collected from the CA-Qfo flux site in 2009 and 2010. Snow-melting periods were estimated based on Phenocam imagery.

Similar effects were seen for the other greenness indices (NIRv and kNDVI), with much of the seasonal change attributable to changes in snow cover rather than changes in vegetation associated with GPP (Fig. 4). Snow had the opposite effect on CCI; snowmelt reversed the sign of the relationship between GPP and CCI (from positive to negative) (Fig. 4), greatly reducing the seasonal variation in CCI and its correlation with GPP.

Due to the effects of snow on these reflectance-based indices (Figs. 2–4), removal of snow-affected data clearly changed the relationship between GPP and vegetation indices in each site, expressed as the correlations between daily GPP and vegetation indices for the 47 sites (Fig. 5). The high accuracy of snow identification using binary SVM classification (average classification accuracy = 0.968) and low errors in fitting vegetation indices seasonal curves indicated high confidence in the snow removal algorithm (Table S1 in the supplemental materials). Before snow correction, all of the NDVI-based indices were more strongly correlated with GPP than CCI, which had a notably weaker correlation with GPP (Fig. 5). After snow removal, the correlation between GPP and CCI was enhanced, while the correlation between GPP and NDVI-based indices (NDVI, NIRv, and kNDVI) decreased slightly (Fig. 5). After snow correction, we also noticed less among site variations between GPP-CCI correlation than GPP-NDVI based indices correlations (Fig. 5).

Snow removal clearly improved the ability of CCI to track GPP change for the subarctic and subtropical sites (Table 1 and Fig. 6). Overall, CCI and NIRv yielded stronger relationships with GPP than NDVI and kNDVI (Fig. 6). Strong relationships between GPP and NDVI based indices were found for subarctic and high elevation sites that belong to the ecoregion of Northwestern forested mountains, likely because of a large contribution of the background annual vegetation, which could enhance the relationship between overall ecosystem GPP and greenness indices. For most Mediterranean sites, CCI outperformed NDVI based indices in tracking GPP phenology, expressed as stronger correlation with daily GPP (Fig. 6).

Strong correlations were found between APAR and vegetation indices, except for the mid-latitude sites (Fig. 6). For most of the sites, NIRv showed the strongest correlation with APAR among three tested vegetation indices, except for Mediterranean and humid subtropical (Eastern temperate forests) sites (Fig. 6). There were only relatively weak correlations between LUE and vegetation indices, and these correlations were strongest for the high latitude boreal forests. For most of the sites, CCI showed a slightly better relationship with LUE than the NDVI-based indices, largely because fewer sites reported CCI having low (negative) correlations, unlike the NDVI-based indices.

Correlation between GPP and vegetation indices varied with ecoregion (Fig. 7). Overall, vegetation indices performed best at monitoring GPP at the northern boreal and taiga sites with a subarctic climate and at the Eastern temperate sites with a humid subtropical climate, but (except for CCI) worked poorly at Temperate Sierra sites. Unlike the NDVI-based indices, CCI performed more consistently across sites, and lacked sites with negative CCI-GPP correlations. Vegetation indices performed better at the Northern forests and Taiga than Northwestern forests mountains, Eastern temperate forests, Marine west coast forests, and Temperate Sierras. Relationships between GPP and CCI and between GPP and NIRv were stronger than those between GPP and NDVI in Marine west coast forests. NDVI based indices, including NIRv, were

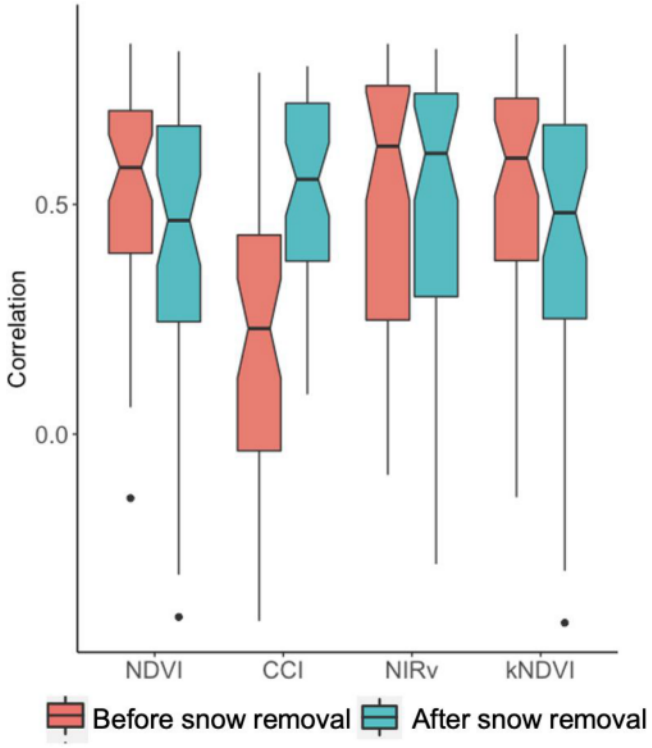

Fig. 5. Snow removal affected the correlations (Pearson correlation coefficients) between daily GPP and vegetation indices (NDVI, CCI, NIRv, and kNDVI). Data from all the 47 sites were used and correlation was calculated for each site separately. The line in the middle of each box indicates the median value. The lower and upper hinges correspond to the first and third quartiles (the 25th and 75th percentiles) and data beyond 1.5 times of distance between the first and third quartiles from the lower and upper hinges are plotted as individual points. The medians are roughly significantly different at a 95% confidence level, if the notches do not overlap (McGill et al., 1978).

poorly correlated with GPP in the Temperate sierras. The largest variations in the GPP – VI relationships occurred in the Northwestern forested mountains, which covered four different climate classes (Fig. 7 and Table 1).

We further explored how relationships between GPP and snow corrected vegetation indices varied among climate classes within Eastern temperate forest and Northwestern forested mountains, both of which cover multiple climate classes (Table 1 and Fig. 8). All vegetation indices were able to track GPP in warm summer continental (Dfb) and dry continental (Dsc) sites. Relationship between GPP and CCI was stronger than those between GPP and NDVI-based indices in Mediterranean sites with dry and warm summer (Csb). The relationship between GPP and NDVI based indices was stronger than that between GPP and CCI in subarctic (Dfc) Northwestern forested mountains. As in the comparison across ecoregions (Fig. 7), CCI performed more consistently across climate classes than NDVI-based indices, and it did not exhibit any sites with negative CCI-GPP correlations (Fig. 8).

4. Discussion

Our study combined flux data and MODIS-derived vegetation indices over 47 North American evergreen forest sites to evaluate the relationships between GPP and vegetation indices, and the confounding effects of snow on these relationships. We greatly expanded the number of sites compared to earlier CCI studies (Rahman et al., 2004; Drolet et al., 2008; Gamon et al., 2016; Middleton et al., 2016). We also extended the analysis well beyond boreal forests to many evergreens across ecoregions and climate classes to test the application of CCI and other VIs in tracking GPP in evergreen forests across a much wider geographic range than most previous studies. Our results revealed that reflected light from snow strongly influenced all vegetation indices, and their correlations with GPP. Prior to snow correction, the NDVI-based indices performed better than CCI in monitoring GPP of evergreen forests, but this was partly due to artifacts of snow, which affected VIs unevenly. After snow correction, the correlation between CCI and GPP was largely enhanced. Our results also showed that correlations between GPP and CCI vs. NDVI-based indices are driven by different factors in the light use efficiency model. The strong performance of CCI was presumably due to its sensitivity to seasonal pigment changes (Gamon et al., 2016; Wong et al., 2020), while NDVI-based indices were more sensitive to APAR and leaf development of deciduous components in the evergreen forest. We also found that the relationship between GPP and vegetation indices varied among ecoregions and climate classes, presumably due to the varying constraints on GPP and stand composition across biomes.

4.1. Effects of snow cover and snow melting on MODIS VIs

Different vegetation indices were affected differently by snow cover, indicating contradictory and confounding effects of snow on these indices (Figs. 4 and 5). For example, snow tended to exaggerate the seasonal trends in NDVI, kNDVI and NIRv, but suppress the seasonal trends in CCI. Although snow increased reflectance across the whole visible (VIS) - near infrared (NIR) region, it decreased the difference between VIS and NIR bands and altered reflectance values of VIS wavelengths, leading to abrupt decreases in NDVI-based indices and an increase in CCI as has also been reported in a recent experimental study (Wang et al., 2023). Without accounting for snow cover, NDVI-based indices could suggest (incorrectly) a rapid loss and relative sudden emergence of green foliage in the winter for evergreens due to changes in snow cover alone. Being inversely impacted by snow (relative to NDVI), CCI increases due to snow in wintertime that are comparable to growing season maxima (Fig. 2) could erroneously suggest a sudden "turning on" of photosynthesis that in the middle of winter for evergreens. Thus, snow increased the seasonal variation in NDVI-based indices, exaggerating the correlation between GPP and NDVI. By contrast, snow decreased the seasonal variation in CCI, greatly reducing the correlation with GPP.

Eliminating the contamination of vegetation indices due to snow revealed the true baseline of the vegetation response and enabled improved evaluation of seasonal patterns associated with biological changes affecting GPP (Huemmrich et al., 2021). Snow – and hence snow correction – had a particularly strong influence in the early spring when rapid changes occurred in both GPP and snow cover (Fig. 2). In accord with previous studies (Eklundh et al., 2011; Springer et al., 2017), the largest and fastest NDVI increases happened during snow melt (Figs. 2 and 4). This effect was an artifact of snow melt, and not a direct effect of vegetation phenology or physiological change. This documentation of severe artifacts in the VI-GPP relationships has important implications for attempts to monitor long-term GPP trends from satellites, as most studies that use reflectance-based vegetation indices do not account for snow cover, and a large part of the signal falsely attributed to GPP trends can be an artifact of changing snow cover (Gamon et al., 2013; Myers-Smith et al., 2020; Shen et al., 2014).

4.2. VIs provided complementary information about photosynthetic phenology

The complementarity hypothesis (Gamon 2015; Gamon et al., 2016) argues that different vegetation indices provide complementary information about plant photosynthetic activities. NDVI follows canopy development (mainly in annual and deciduous plants) while CCI is sensitive to seasonal pigment changes particularly the relative levels of chlorophyll and carotenoid pigments (Gamon et al., 2016; Wong et al., 2020), both of which can have an important influence on GPP (Springer

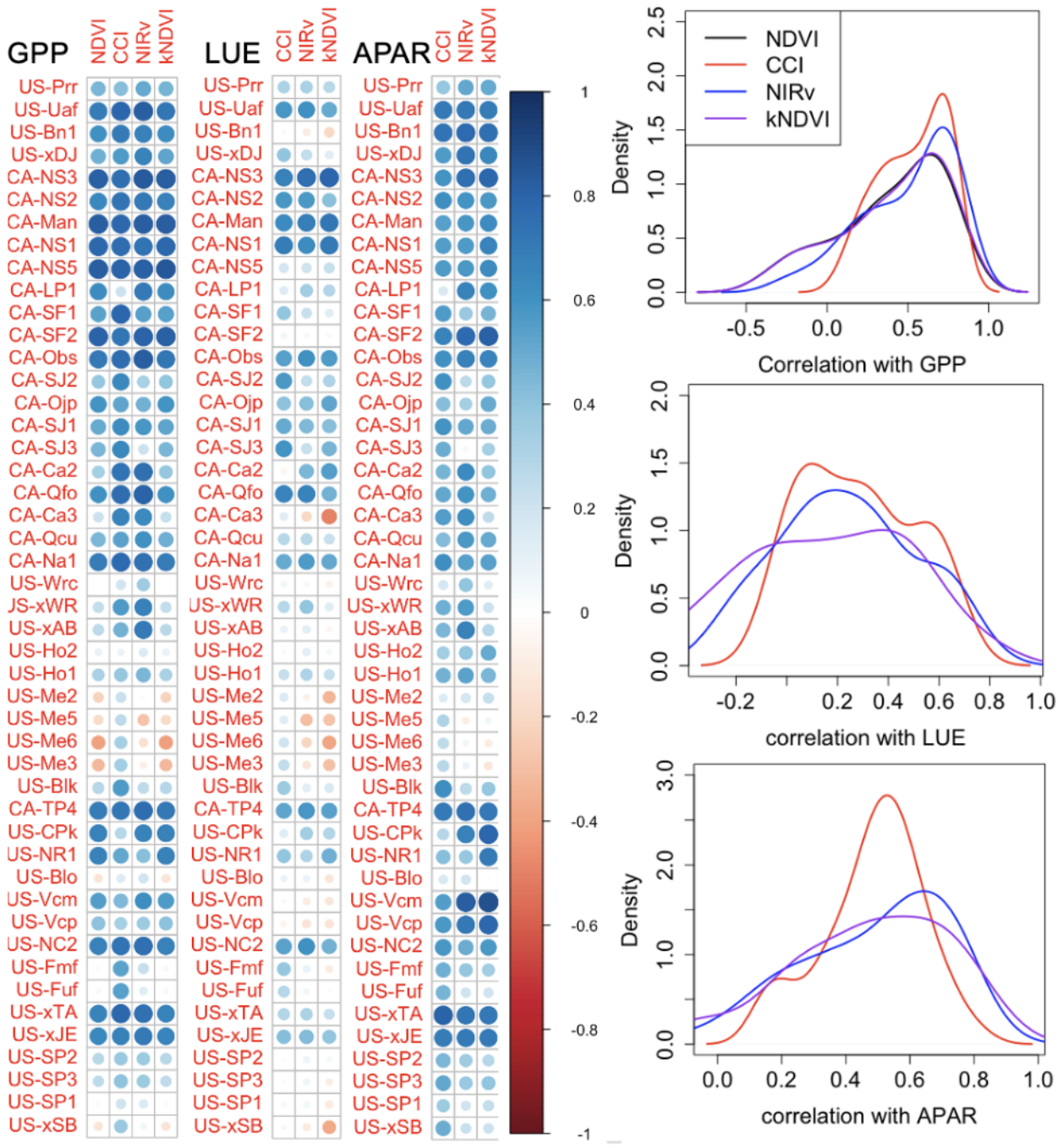

Fig. 6. Correlations (Pearson correlation coefficient) between GPP, LUE, and APAR and snow corrected vegetation indices. Size and color of circles indicate the Pearson correlation coefficient. Sites listed on the left were sorted by latitude (from North to South). Ecoregions and climate class of each site are summarized in Table 1. Correlations between NDVI and APAR and LUE were not calculated, because NDVI was used to derive APAR and thus LUE.

et al., 2017; Wong et al., 2020). Carotenoid pigments often serve as photoprotective and photoregulatory pigments. Presumably, because carotenoid pigments serve a particularly strong photoprotective role in evergreens, CCI is also more sensitive to LUE than the NDVI-based indices (Fig. 6). A history of research has shown that seasonal shifts in photosynthetic and photoregulatory pigments are important in regulating seasonal photosynthetic activity, particularly under extreme temperatures (Wong and Gamon, 2015; Magney et al., 2019; Walter-McNeill et al., 2021). The balance of these physiological and structural factors and their influence on GPP changes with vegetation type (Gamon, 2015; Garbulsky et al., 2011), and this affects the relationships between GPP and vegetation indices in different ways depending upon the index and the particular biome.

The weak correlation between GPP and NDVI for most of the evergreen forests tested is undoubtedly due to NDVI's sensitivity to green canopy structure (which has little seasonal change in evergreens) along with its insensitivity to subtle changes in physiology associated with pigments and seasonal photosynthetic capacity change in evergreens. Because CCI is more sensitive to the seasonal dynamics in pigments, a good indicator of the regulation of photosynthetic light reactions, it appears to be a more sensitive indicator of LUE and evergreen GPP phenology than greenness-based indices like NDVI, as has previously been reported (Gamon et al., 2016; Springer et al., 2017). In contrast, greenness-based indices like NDVI can provide good estimates of radiation absorbed by green canopy material (APAR) and are sensitive to the contributions of leaf development and senescence to overall optical

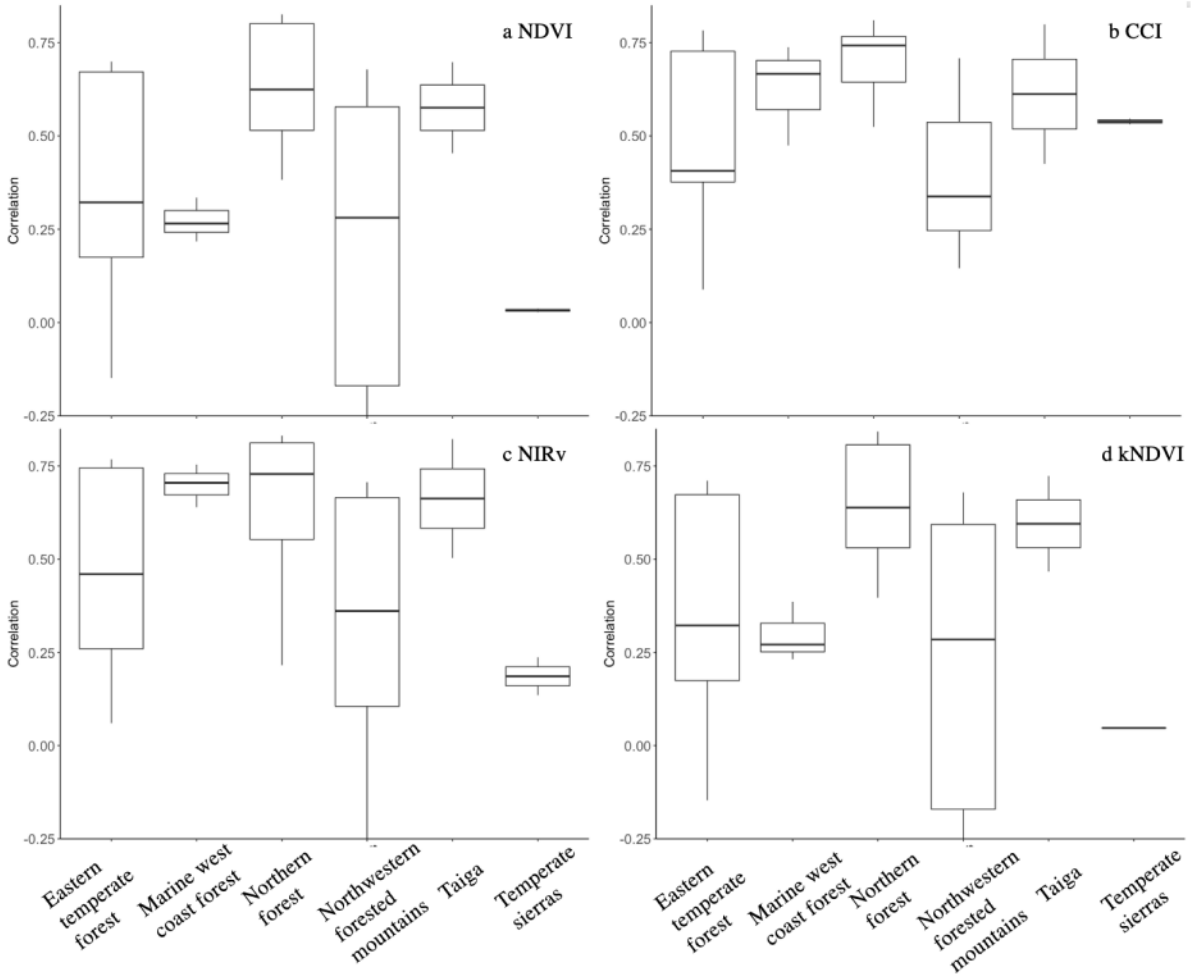

Fig. 7. Correlations between GPP and snow corrected vegetation indices (NDVI, CCI, NIRv, and kNDVI) by Level-1 ecoregions. The line in the middle of each box indicates the median value. The lower and upper hinges correspond to the first and third quartiles (the 25th and 75th percentiles).

signals in annual and deciduous species and understory that could influence the reflectance in northern sites (Ikawa et al., 2015), and thus of potential photosynthetic activity (Gamon et al., 1995, 2016; Wong et al., 2020). CCI also had strong correlations with APAR (Fig. 6). This might be because CCI was sensitive to both adjustment of pigments in the spring and fall as well as to canopy structural change such as needle expansion and shoot elongation (Springer et al., 2017). To track actual photosynthetic activity (and GPP), additional pigment information provided by CCI appears to be very useful, and this can help explain the higher correlation between CCI and LUE relative to the other vegetation indices (Fig. 6). Combining CCI and NIRv by assuming that these two indices may represent light use efficiency and APAR in the conventional LUE model respectively, could lead to stronger relationship with GPP than using each index alone (Wong et al., 2022). We calculated an index by multiplying normalized CCI (to the [0, 1] range to eliminate the effects of negative values) with NIRv, which led to a slight increase in the correlation with GPP (Figure S7 in the supplemental materials), suggesting that this may be a promising direction for future study. In addition, correction for sun-view geometry and shadow fraction in the MODIS data, which were not attempted here, may further improve the relationship between CCI and GPP (Drolet et al., 2008; Middleton et al., 2016).

4.3. GPP-VI relationships varied among ecoregions

The distribution and growth of evergreen forests are influenced by climate (temperature and precipitation), and these effects vary among ecoregions. Evergreen forests can also vary in the proportion of annual and deciduous species present, which can vary with disturbance and succession (Wells et al., 2020). Evergreen and deciduous species also differ in their optical responses to snow and their GPP phenology (Wang et al., 2023). These factors undoubtedly contribute to the geographic variation in the relationships between GPP and VIs (Fig. 7). Forest growth and distribution are limited by long winters with cold temperature and short daylength for taiga, northern forests and subarctic sites in the northwest forested mountains (Seyednasrollah et al., 2021). Besides being affected by temperature and light regime, forest distribution and growth are affected by soil hydrology. Forest growth can be limited by the water holding capacity of sandy soils, such as those from the Great Lakes region or eastern North America, which quickly become dry during periods of drought (Arain et al., 2022; Arain and Restrepo--Coupe, 2005) and some of the jack pine (*Pinus banksiana*) forests in the boreal region (Dietrich et al., 2016; McCollum and Ibáñez, 2020). In regions with pronounced seasonal GPP patterns, including taiga, northern forests and other subarctic sites, all four vegetation indices were able to track seasonal GPP change (Figs. 6 and 7). The relatively low correlation between vegetation indices and GPP for two east coastal forest sites (US-Ho1 and US-Ho2) was due to limited GPP data (mainly in the fall) caused by failed daytime partitioning for most of the data. Strong relationships between VIs and GPP derived from nighttime partitioning were achieved for these two sites (Figure S4 in the supplemental materials). This indicates that flux partitioning method can also be a source of error affecting GPP-VI relationships.

The marine west coast forest sites (CA-Ca2 and CA-Ca3) are located

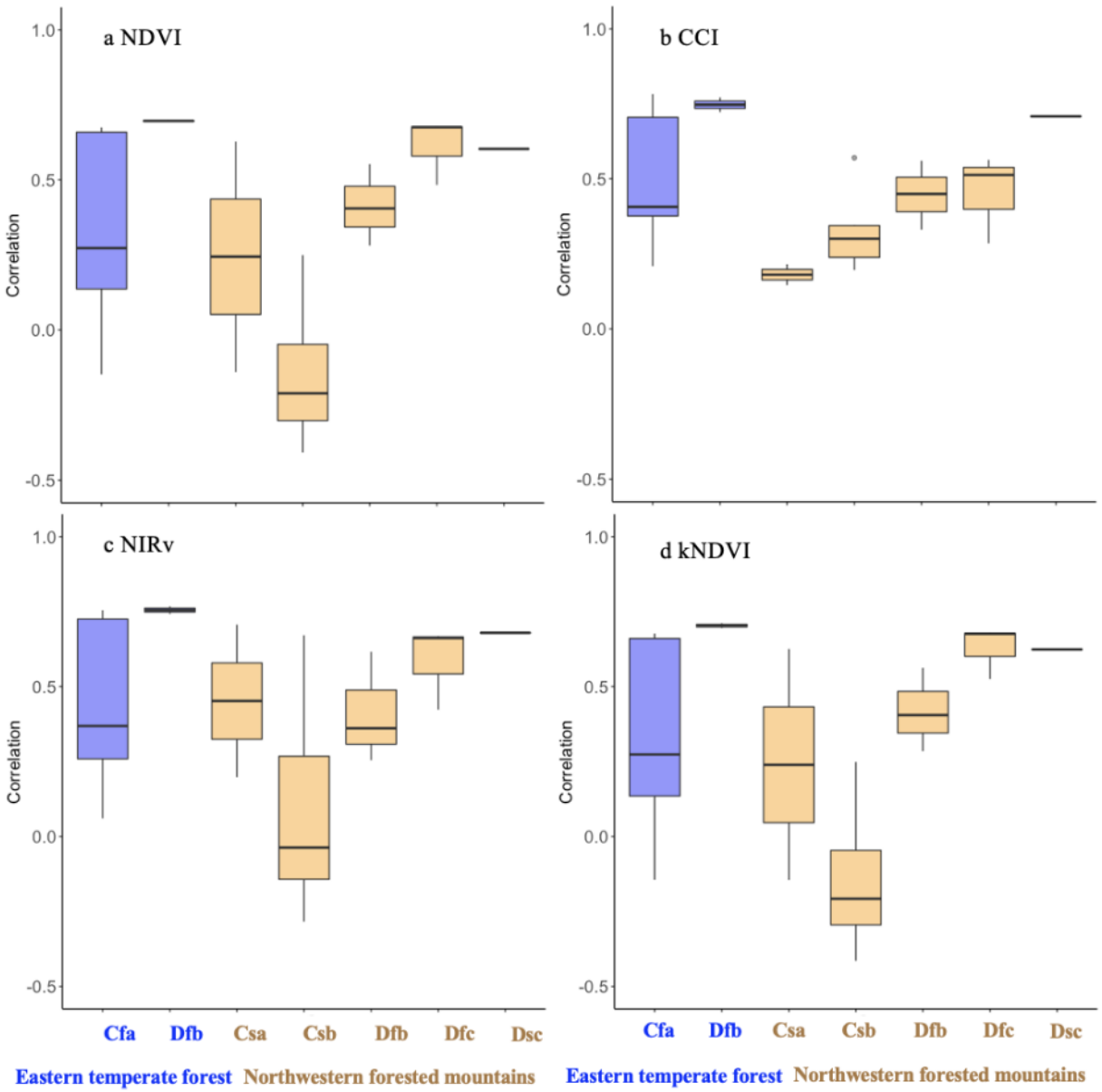

Fig. 8. Correlations between GPP and snow corrected vegetation indices (NDVI, CCI, NIRv, and kNDVI) by Köppen Climate Class within Eastern temperate forest and Northwestern forested mountains. The line in the middle of each box indicates the median value. The lower and upper hinges correspond to the first and third quartiles (the 25th and 75th percentiles).
Cfa: Humid subtropical (mild with no dry season, hot summer); Dfb: Warm summer continental (significant precipitation in all seasons); Csa: Mediterranean (mild with dry, hot summer); Csb: Mediterranean (mild with dry, warm summer); Dfc: Subarctic (severe winter, no dry season, cool summer); Dsc: Dry continental (cool summer).

in the wettest climate in North America and are dominated by dense Douglas-fir, hemlock and cedar. In this case, the contribution of understory deciduous plants to reflectance can often be negligible, except following fire, harvesting or in early forest succession when annuals or deciduous vegetation species dominate (Humphreys et al., 2006). Thus, CCI was able to track the GPP phenology for these sites due to its sensitivity to seasonal pigment changes while NDVI and kNDVI exhibited little sensitivity to seasonal changing GPP (Fig. 6, Gamon et al., 2016).

For Temperate Sierras (US-Fmf and US-Fuf) and some other Mediterranean sites (US-Me2, US-Me3, US-Me5, and US-Me6), where the climate features dry and warm summer and wet winter, strong correlations were only found between GPP and CCI, with all the NDVI based indices failing to track GPP phenology (Fig. 7). In some Mediterranean sites, GPP is restricted by summer drought and associated photosynthetic downregulation in hot summer conditions (Goulden et al., 2012; Kelly and Goulden, 2016), and vary with forest management and disturbance, such as fire treatment (Kolb et al., 2013). In accordance with previous study at sites US-Fmf and US-Fuf (Kolb et al., 2013), in a year with late summer drought, NDVI based indices showed little capability to monitor the overall seasonal GPP change (Fig. 6). Moderate correlation ($r = 0.5$) was found between GPP and CCI among all the years and management treatments, perhaps because of the additional sensitivity of CCI to pigment signals indicating periods of photosynthetic (GPP) downregulation (Fig. 6). A large body of literature suggests that carotenoid-based indices may be responsive to drought-induced declines in photosynthetic activity (Suárez et al., 2008, 2010; Zarco-Tejada et al., 2012), supporting the good correlation between CCI and GPP in these systems.

4.4. Disturbance impacts

Besides climate effects, the overall ecosystem photosynthesis and carbon uptake of forests are affected by disturbance, such as drought, fire and pests (Amiro et al., 2010; Kurz et al., 2013; Xu et al., 2020). Such disturbances are becoming more frequent in many regions, altering the successional state of forests, and affecting both the distribution of vegetation types and presumably the links between vegetation indices and GPP (Zhang et al., 2016; Sarmah et al., 2021). In this study, NIRv exhibited the strongest correlation with GPP for the site CA-LP1, which is a lodgepole pine (*Pinus contorta*) stand that has been severely affected by mountain pine beetle (MPB, *Dendroctonus, ponderosae*) since the early 2000s. This is likely due to NIRv s sensitivity to green canopy structure. While most of the mature pine canopy was killed, residual vegetation, including younger conifer trees and broadleaf dominated understory, contributed to the overall ecosystem net photosynthesis (Bowler et al., 2012; Emmel et al., 2014). However, the yellow to red dead tree foliage that was caused by beetle attack can, for a few years post-disturbance, affect the vegetation indices and presumably influence the correlation between GPP and CCI at this site. A systematic evaluation of impacts of disturbance on relationships between GPP and vegetation indices is beyond the scope of this study, but further attention is required when estimating GPP using vegetation indices for disturbance influenced sites.

4.5. Next generation satellites

The results of this study indicate that combinations of structurally-based (NDVI-based) with pigment-based (e.g. CCI) indices can provide improved estimation of GPP, as has been amply demonstrated from a history of proximal remote sensing. Such combined approaches would benefit from additional attention to snow correction as demonstrated here. However, due to the orbital drift of Terra and Aqua satellites, the global CCI observation capability derived from MODIS data will likely be limited at some point in the near future. The Visible Infrared Imaging Radiometer Suite (VIIRS) instrument flying on the Suomi National Polar-orbiting Partnership satellite, intended to be the continuation of MODIS, did not retain the 531 nm band needed for calculation of CCI. Current hyperspectral satellites such as PRISMA (Cogliati et al., 2021; Stefano et al., 2013) and EnMAP (Guanter et al., 2015) do not have enough temporal coverage or are not free for public access. One option is the Second-Generation Global Imager (SGLI) on-board on the Global Change Observation Mission Climate (GCOM-C), which provides surface reflectance at 531 nm (Akitsu and Nasahara, 2022). Yet to be tested, SGLI-based measurements might be able to provide the ability to detect pigment-based GPP estimations through global PRI and CCI products until new hyperspectral satellites, such as NASA Surface Biology and Geology (Cawse-Nicholson et al., 2021) and ESA Fluorescence Explorer (Drusch et al., 2017) missions, are launched. Thus, it is likely that gaps in global coverage of critical VIs will occur in the near future, affecting our ability to assess GPP from reflectance-based methods due to limited satellite coverage.

5. Conclusions

The satellite-derived vegetation indices commonly used to monitor terrestrial ecosystem photosynthesis phenology are highly sensitive to snow cover. Consequently, the performance of these indices in tracking global GPP phenology is confounded by snow, a topic which has received only limited attention (e.g., Myers-Smith et al., 2020) despite the heavy use of vegetation indices in global GPP studies. During the spring transition, snow melt greatly exaggerated the apparent correlation between GPP and NDVI-based vegetation indices while reversing the correlation between GPP and CCI. After snow removal, strong relationships were found between GPP and CCI and NIRv, with slightly higher correlations between GPP and CCI for most of the sites, presumably due to the sensitivity of CCI to seasonal pigment change associated with changing photosynthetic activity and photoprotection. The relationship between GPP and vegetation indices varied among geographical regions, ecoregions and climate classes. The GPP-VI relationship was likely further affected by disturbance history and the exact composition of functionally distinct vegetation types (e.g. annuals, deciduous and evergreen). For regions with clear seasonal GPP patterns, all vegetation indices were able to track GPP phenology to some degree. Among all the ecoregions (climate classes), the strongest relationships between GPP and vegetation indices were found for the subarctic sites, while weak relationships between were found for the Mediterranean sites, where daily GPP exhibited moderate correlation with CCI. The large snow cover artifacts and complementary vegetation index responses reported here should be considered in any large-scale studies of GPP using optical satellites (e.g. MODIS) and illustrate the limitations of deriving global GPP estimates based on any single vegetation index.

Declaration of Competing Interest

The authors declare that they have no known competing financial interests or personal relationships that could have appeared to influence the work reported in this paper.

Data availability

All the data used in this study are open to public.

Acknowledgments

We thank Dr. Alexei Lyapustin s team for making the MODIS MAIAC data available. This work was supported by the Macrosystems Biology and NEON-Enabled Science (award 1926090) and Division of Environmental Biology programs (award 1929709) to DRB and JAG and NASA Arctic-Boreal Vulnerability Experiment grant (NNX15AT78A) to JAG. MU was supported by the Arctic Challenge for Sustainability II (ArCS II; JPMXD1420318865) project.

We are grateful to the worldwide flux tower community for publicly sharing data, including AmeriFlux (funding provided by the U.S. Department of Energy Office of Science), FLUXNET2015 (supported by European Union H2020 projects and U.S. Department of Energy Office of Science) and the National Ecological Observatory Network (supported by the National Science Foundation). We thank our many collaborators, including site PIs and technicians, for their efforts in support of PhenoCam. The development of PhenoCam has been funded by the Northeastern States Research Cooperative, NSF s Macrosystems Biology program (awards EF-1065029 and EF-1702697), and DOE s Regional and Global Climate Modeling program (award DE-SC0016011). The authors acknowledge constructive comments from two anonymous reviewers that greatly improved the manuscript.

Supplementary materials

Supplementary material associated with this article can be found, in the online version, at doi:10.1016/j.agrformet.2023.109600.

References

Akitsu, T.K., Nasahara, K.N., 2022. *In-situ* observations on a moderate resolution scale for validation of the global change observation mission-climate ecological products: the uncertainty quantification in ecological reference data. Int. J. Appl. Earth Obs. Geoinf. 107, 102639 https://doi.org/10.1016/j.jag.2021.102639.

Amiro, B.D., Barr, A.G., Barr, J.G., Black, T.A., Bracho, R., Brown, M., Chen, J., Clark, K. L., Davis, K.J., Desai, A.R., Dore, S., Engel, V., Fuentes, J.D., Goldstein, A.H., Goulden, M.L., Kolb, T.E., Lavigne, M.B., Law, B.E., Margolis, H.A., Martin, T., McCaughey, J.H., Misson, L., Montes-Helu, M., Noormets, A., Randerson, J.T., Starr, G., Xiao, J., 2010. Ecosystem carbon dioxide fluxes after disturbance in forests of North America. J. Geophys. Res. Biogeosci. 115 https://doi.org/10.1029/2010JG001390.

Amiro B.D., (2016), AmeriFlux BASE CA-man manitoba - northern old black spruce (former BOREAS northern study area), Ver. 2-1, AmeriFlux AMP, (dataset). 10.17190/AMF/1245997.

Amiro B.D., (2019), AmeriFlux BASE CA-SF2 saskatchewan - Western Boreal, forest burned in 1989, Ver. 3-5, AmeriFlux AMP, (dataset). 10.17190/AMF/1246007.

Amiro B.D., (2020), AmeriFlux BASE CA-SF1 saskatchewan - Western Boreal, forest burned in 1977, Ver. 2-5, AmeriFlux AMP, (dataset). 10.17190/AMF/1246006.

Ammer, C., 2019. Diversity and forest productivity in a changing climate. New Phytol. 221, 50 66. https://doi.org/10.1111/nph.15263.

Arain, M.A., Restrepo-Coupe, N., 2005. Net ecosystem production in a temperate pine plantation in southeastern Canada. Agric. For. Meteorol. 128, 223 241. https://doi.org/10.1016/j.agrformet.2004.10.003.

Arain, M.A., Xu, B., Brodeur, J.J., Khomik, M., Peichl, M., Beamesderfer, E., Restrepo-Couple, N., Thorne, R., 2022. Heat and drought impact on carbon exchange in an age-sequence of temperate pine forests. Ecol. Process. 11 https://doi.org/10.1186/s13717-021-00349-7.

Arain M.A. (2018), AmeriFlux BASE CA-TP4 Ontario - Turkey point 1939 plantation White Pine, Ver. 4-5, AmeriFlux AMP, (dataset). 10.17190/AMF/1246012.

Badgley, G., Field, C.B., Berry, J.A., 2017. Canopy near-infrared reflectance and terrestrial photosynthesis. Sci. Adv. 3, e1602244 https://doi.org/10.1126/sciadv.1602244.

Barr A., Black T.A., (2018), AmeriFlux BASE CA-SJ2 Saskatchewan - Western Boreal, Jack Pine forest harvested in 2002, Ver. 2-5, AmeriFlux AMP, (Dataset). 10.17190/AMF/1436321.

Barr A. (2018), AmeriFlux BASE CA-SJ1 saskatchewan - Western Boreal, Jack Pine forest harvested in 1994, Ver. 1-5, AmeriFlux AMP, (Dataset). 10.17190/AMF/1436320.

Barr A. (2018), AmeriFlux BASE CA-SJ3 saskatchewan - Western Boreal, Jack Pine forest harvested in 1975 (BOREAS Young Jack Pine), Ver. 2-5, AmeriFlux AMP, (Dataset). 10.17190/AMF/1436322.

Black T.A., (2016), AmeriFlux BASE CA-Obs Saskatchewan - Western Boreal, Mature Black Spruce, Ver. 1-1, AmeriFlux AMP, (Dataset). 10.17190/AMF/1375198.

Black T.A., (2018), AmeriFlux BASE CA-Ca2 British Columbia - Clearcut Douglas-fir stand (harvested winter 1999/2000), Ver. 1-5, AmeriFlux AMP, (Dataset). 10.17190/AMF/1480301.

Black T.A., (2019), AmeriFlux BASE CA-Ojp Saskatchewan - Western Boreal, Mature Jack Pine, Ver. 2-5, AmeriFlux AMP, (Dataset). 10.17190/AMF/1375199.

Black T.A., (2022), AmeriFlux BASE CA-LP1 British Columbia - Mountain pine beetle-attacked lodgepole pine stand, Ver. 3-5, AmeriFlux AMP, (Dataset). 10.17190/AMF/1660337.

Black T.A., (2023), AmeriFlux BASE CA-Ca3 British Columbia - Pole sapling Douglas-fir stand, Ver. 5-5, AmeriFlux AMP, (Dataset). 10.17190/AMF/1480302.

Blanken P., Monson R., Burns S., Bowling D., Turnipseed A. (2022), AmeriFlux BASE US-NR1 Niwot Ridge Forest (LTER NWT1), Ver. 19-5, AmeriFlux AMP, (Dataset). 10.17190/AMF/1246088.

Bonan, G.B., 2008. Forest and climate change: forcings, feedbacks, and the climate benefits of forests. Science 320, 1444 1449.

Boser, B.E., Vapnik, V.N., Guyon, I.M., 1992. Training algorithm margin for optimal classifiers. Perception 144 152.

Bourque C. (2018), AmeriFlux BASE CA-Na1 new brunswick - 1967 Balsam Fir - Nashwaak Lake Site 01 (Mature balsam fir forest), Ver. 1-5, AmeriFlux AMP, (Dataset). 10.17190/AMF/1436319.

Bowler, R., Fredeen, A.L., Brown, M., Andrew Black, T., 2012. Residual vegetation importance to net CO_2 uptake in pine-dominated stands following mountain pine beetle attack in British Columbia, Canada. For. Ecol. Manag. 269, 82 91. https://doi.org/10.1016/j.foreco.2011.12.011.

Bowling, D.R., Logan, B.A., Hufkens, K., Aubrecht, D.M., Richardson, A.D., Burns, S.P., Anderegg, W.R.L., Blanken, P.D., Eiriksson, D.P., 2018. Limitations to winter and spring photosynthesis of a Rocky Mountain subalpine forest. Agric. For. Meteorol. 252, 241 255. https://doi.org/10.1016/j.agrformet.2018.01.025.

Bracho, R., Martin, T. (2016a), AmeriFlux BASE US-SP2 Slashpine-Mize-clearcut-3yr, regen, Ver. 3-1, AmeriFlux AMP, (Dataset). https://doi.org/10.17190/AMF/1246101.

Bracho, R., Martin, T. (2016b), AmeriFlux BASE US-SP3 Slashpine-Donaldson-mid-rot-12yrs, Ver. 3-1, AmeriFlux AMP, (Dataset). doi:10.17190/AMF/1246102.

Bracho, R., Martin, T. (2016c), AmeriFlux BASE US-SP1 Slashpine-Austin Cary- 65yrs nat regen, Ver. 4-1, AmeriFlux AMP, (Dataset). https://doi.org/10.17190/AMF/1246100.

Camps-Valls, G., Campos-Taberner, M., Moreno-Martínez, A., Walther, S., Duveiller, G., Cescatti, A., Mahecha, M.D., Munoz-Marí, J., García-Haro, F.J., Guanter, L., Jung, M., Gamon, J.A., Reichstein, M., Running, S.W., 2021. A unified vegetation index for quantifying the terrestrial biosphere. Sci. Adv. 7, 1 11. https://doi.org/10.1126/sciadv.abc7447.

Cawse-Nicholson, K., Townsend, P.A., Schimel, D., Assiri, A.M., Blake, P.L., Buongiorno, M.F., Campbell, P., Carmon, N., Casey, K.A., Correa-Pabon, R.E., Dahlin, K.M., Dashti, H., Dennison, P.E., Dierssen, H., Erickson, A., Fisher, J.B., Frouin, R., Gatebe, C.K., Gholizadeh, H., Gierach, M., Glenn, N.F., Goodman, J.A., Griffith, D.M., Guild, L., Hakkenberg, C.R., Hochberg, E.J., Holmes, T.R.H., Hu, C., Hulley, G., Huemmrich, K.F., Kudela, R.M., Kokaly, R.F., Lee, C.M., Martin, R., Miller, C.E., Moses, W.J., Muller-Karger, F.E., Ortiz, J.D., Otis, D.B., Pahlevan, N., Painter, T.H., Pavlick, R., Poulter, B., Qi, Y., Realmuto, V.J., Roberts, D., Schaepman, M.E., Schneider, F.D., Schwandner, F.M., Serbin, S.P., Shiklomanov, A. N., Stavros, E.N., Thompson, D.R., Torres-Perez, J.L., Turpie, K.R., Tzortziou, M., Ustin, S., Yu, Q., Yusup, Y., Zhang, Q., 2021. NASA s surface biology and geology designated observable: a perspective on surface imaging algorithms. Remote Sens. Environ. 257 https://doi.org/10.1016/j.rse.2021.112349.

Cheng, R., Magney, T.S., Dutta, D., Bowling, D.R., Logan, B.A., Burns, S.P., Blanken, P.D., Grossmann, K., Lopez, S., Richardson, A.D., Stutz, J., Frankenberg, C., 2020. Decomposing reflectance spectra to track gross primary production in a subalpine evergreen forest. Biogeosciences 17, 4523 4544. https://doi.org/10.5194/bg-17-4523-2020.

Cogliati, S., Sarti, F., Chiarantini, L., Cosi, M., Lorusso, R., Lopinto, E., Miglietta, F., Genesio, L., Guanter, L., Damm, A., Perez-Lopez, S., Scheffler, D., Tagliabue, G., Panigada, C., Rascher, U., Dowling, T.P.F., Giardino, C., Colombo, R., 2021. The PRISMA imaging spectroscopy mission: overview and first performance analysis. Remote Sens. Environ. 262 https://doi.org/10.1016/j.rse.2021.112499.

Demmig-Adams, B., Adams, W.W., 1996. The role of xanthophyll cycle carotenoids in the protection of photosynthesis. Trends Plant Sci. 1, 21 26. https://doi.org/10.1016/S1360-1385(96)80019-7.

Dial, R.J., Maher, C.T., Hewitt, R.E., Sullivan, P.F., 2022. Sufficient conditions for rapid range expansion of a boreal conifer. Nature 608, 546 551. https://doi.org/10.1038/s41586-022-05093-2.

Dietrich, R., Bell, F.W., Silva, L.C.R., Cecile, A., Horwath, W.R., Anand, M., 2016. Climatic sensitivity, water-use efficiency, and growth decline in boreal jack pine (Pinus banksiana) forests in Northern Ontario. J. Geophys. Res. Biogeosci. 121, 2761 2774. https://doi.org/10.1002/2016JG003440.

Dore S., Kolb T. (2019), AmeriFlux BASE US-Fmf Flagstaff - Managed Forest, Ver. 6-5, AmeriFlux AMP, (Dataset). 10.17190/AMF/1246050.

Dore S., Kolb T. (2019), AmeriFlux BASE US-Fuf Flagstaff - Unmanaged Forest, Ver. 6-5, AmeriFlux AMP, (Dataset). 10.17190/AMF/1246051.

Dozier, J., Green, R.O., Nolin, A.W., Painter, T.H., 2009. Interpretation of snow properties from imaging spectrometry. Remote Sens. Environ. 113 (SUPPL. 1), S25 S37. https://doi.org/10.1016/j.rse.2007.07.029.

Drolet, G.G., Middleton, E.M., Huemmrich, K.F., Hall, F.G., Amiro, B.D., Barr, A.G., Black, T.A., McCaughey, J.H., Margolis, H.A., 2008. Regional mapping of gross light-use efficiency using MODIS spectral indices. Remote Sens. Environ. 112, 3064 3078. https://doi.org/10.1016/j.rse.2008.03.002.

Drusch, M., Moreno, J., Bello, U.D., Franco, R., Goulas, Y., Huth, A., Kraft, S., Middleton, E.M., Miglietta, F., Mohammed, G., Nedbal, L., Rascher, U., Schüttemeyer, D., Verhoef, W., 2017. The fluorescence explorer mission concept ESA s Earth explorer 8. IEEE Trans. Geosci. Remote Sens. 55, 1273 1284.

Eklundh, L., Jin, H., Schubert, P., Guzinski, R., Heliasz, M., 2011. An optical sensor network for vegetation phenology monitoring and satellite data calibration. Sensors. https://doi.org/10.3390/s110807678.

Emmel, C., Paul-Limoges, E., Bowler, R., Black, T.A., Christen, A., 2014. Vertical distribution of carbon dioxide sources and sinks in a recovering mountain pine beetle-attacked lodgepole pine stand. Agric. For. Meteorol. 195 196, 108 122. https://doi.org/10.1016/j.agrformet.2014.04.014.

Ensminger, I., Sveshnikov, D., Campbell, D.A., Funk, C., Jansson, S., Lloyd, J., Shibistova, O., Oquist, G., 2004. Intermittent low temperatures constrain spring recovery of photosynthesis in boreal Scots pine forests. Glob. Change Biol. 10, 995 1008. https://doi.org/10.1111/j.1365-2486.2004.00781.x.

Ewers B., Bretfeld M., Pendall E. (2016), AmeriFlux BASE US-CPk Chimney Park, Ver. 2-1, AmeriFlux AMP, (Dataset). 10.17190/AMF/1246150.

FAO and UNEP, 2020. The State of the World s Forests 2020, Forests, Biodiversity and People. Rome, Italy. 10.4060/ca8642en.

Gamon, J.A., Field, C.B., Goulden, M.L., Griffin, K.L., Hartley, A.E., Joel, G., Penuelas, J., Valentini, R., 1995. Relationships between NDVI, canopy structure, and photosynthesis in three californian vegetation types. Ecol. Appl. 5, 28 41.

Gamon, J.A., Huemmrich, K.F., Stone, R.S., Tweedie, C.E., 2013. Spatial and temporal variation in primary productivity (NDVI) of coastal Alaskan tundra: decreased vegetation growth following earlier snowmelt. Remote Sens. Environ. 129, 144 153. https://doi.org/10.1016/j.rse.2012.10.030.

Gamon, J.A., Kovalchuck, O., Wong, C.Y.S., Harris, A., Garrity, S.R., 2015. Monitoring seasonal and diurnal changes in photosynthetic pigments with automated PRI and NDVI sensors. Biogeosciences 12, 4149 4159. https://doi.org/10.5194/bg-12-4149-2015.

Gamon, J.A., Huemmrich, K.F., Wong, C.Y.S., Ensminger, I., Garrity, S., Hollinger, D.Y., Noormets, A., Penuelas, J., 2016. A remotely sensed pigment index reveals photosynthetic phenology in evergreen conifers. Proc. Natl. Acad. Sci. U. S. A. 113, 13087 13092. https://doi.org/10.1073/pnas.1606162113.

Gamon, J.A., 2015. Optical sampling of the flux tower footprint. Biogeosci. Discuss. 12, 4973 5014. https://doi.org/10.5194/bgd-12-4973-2015.

Garbulsky, M.F., Penuelas, J., Gamon, J.A., Inoue, Y., Filella, I., 2011. The photochemical reflectance index (PRI) and the remote sensing of leaf, canopy and ecosystem radiation use efficiencies: a review and meta-analysis. Remote Sens. Environ. 115, 281 297. https://doi.org/10.1016/j.rse.2010.08.023.

Gelbart, M.A., Snoek, J., Adams, R.P., 2014. Bayesian optimization with unknown constraints. Uncertainty in Artificial Intelligence. In: Proceedings of the 30th Conference, UAI 2014, pp. 250 259.

Gladkova, I., Grossberg, M., Bonev, G., Romanov, P., Shahriar, F., 2012. Increasing the accuracy of MODIS/Aqua snow product using quantitative image restoration technique. IEEE Geosci. Remote Sens. Lett. 9, 740 743. https://doi.org/10.1109/LGRS.2011.2180505.

Goldstein A. (2019), AmeriFlux BASE US-Blo Blodgett Forest, Ver. 4-5, AmeriFlux AMP, (Dataset). 10.17190/AMF/1246032.

Gorelick, N., Hancher, M., Dixon, M., Ilyushchenko, S., Thau, D., Moore, R., 2017. Google Earth engine: planetary-scale geospatial analysis for everyone. Remote Sens. Environ. 202, 18 27. https://doi.org/10.1016/j.rse.2017.06.031.

Goulden, M.L., Anderson, R.G., Bales, R.C., Kelly, A.E., Meadows, M., Winston, G.C., 2012. Evapotranspiration along an elevation gradient in California s Sierra Nevada. J. Geophys. Res. Biogeosci. 117, 1 13. https://doi.org/10.1029/2012JG002027.

Goulden M. (2019), AmeriFlux BASE CA-NS1 UCI-1850 burn site, Ver. 3-5, AmeriFlux AMP, (Dataset). 10.17190/AMF/1245998.
Goulden M. (2019), AmeriFlux BASE CA-NS2 UCI-1930 burn site, Ver. 3-5, AmeriFlux AMP, (Dataset). 10.17190/AMF/1245999.
Goulden M. (2019), AmeriFlux BASE CA-NS3 UCI-1964 burn site, Ver. 3-5, AmeriFlux AMP, (Dataset). 10.17190/AMF/1246000.
Goulden M. (2019), AmeriFlux BASE CA-NS5 UCI-1981 burn site, Ver. 3-5, AmeriFlux AMP, (Dataset). 10.17190/AMF/1246002.
Guanter, L., Kaufmann, H., Segl, K., Foerster, S., Rogass, C., Chabrillat, S., Kuester, T., Hollstein, A., Rossner, G., Chlebek, C., Straif, C., Fischer, S., Schrader, S., Storch, T., Heiden, U., Mueller, A., Bachmann, M., Mühle, H., Müller, R., Habermeyer, M., Ohndorf, A., Hill, J., Buddenbaum, H., Hostert, P., Van Der Linden, S., Leitao, P.J., Rabe, A., Doerffer, R., Krasemann, H., Xi, H., Mauser, W., Hank, T., Locherer, M., Rast, M., Staenz, K., Sang, B., 2015. The EnMAP spaceborne imaging spectroscopy mission for Earth observation. Remote Sens. 7, 8830 8857. https://doi.org/10.3390/rs70708830.
Hassan, R., Scholes, R., Ash, N., 2005. Ecosystems and Human Well-being: Current State and Trends, 1. Island Press, Washington, DC.
Heinsch F.A., Milesi C., Jolly W.M., Bowker C.F., Kimball J.S., Nemani R.R., 2003. User s guide NASA MODIS land algorithm Joseph Glassy.
Hmimina, G., Dufrene, E., Pontailler, J.Y., Delpierre, N., Aubinet, M., Caquet, B., de Grandcourt, A., Burban, B., Flechard, C., Granier, A., Gross, P., Heinesch, B., Longdoz, B., Moureaux, C., Ourcival, J.M., Rambal, S., Saint Andre, L., Soudani, K., 2013. Evaluation of the potential of MODIS satellite data to predict vegetation phenology in different biomes: an investigation using ground-based NDVI measurements. Remote Sens. Environ. 132, 145 158. https://doi.org/10.1016/j.rse.2013.01.010.
Hollinger D. (2021), AmeriFlux BASE US-Ho2 Howland Forest (west tower), Ver. 4-5, AmeriFlux AMP, (Dataset). 10.17190/AMF/1246062.
Hollinger D. (2021), AmeriFlux BASE US-Ho1 Howland Forest (main tower), Ver. 7-5, AmeriFlux AMP, (Dataset). 10.17190/AMF/1246061.
Huemmrich, K.F., Vargas Zesati, S., Campbell, P., Tweedie, C., 2021. Canopy reflectance models illustrate varying NDVI responses to change in high latitude ecosystems. Ecol. Appl. 31 (8), 1 13. https://doi.org/10.1002/eap.2435.
Humphreys, E.R., Black, T.A., Morgenstern, K., Cai, T., Drewitt, G.B., Nesic, Z., Trofymow, J.A., 2006. Carbon dioxide fluxes in coastal Douglas-fir stands at different stages of development after clearcut harvesting. Agric. For. Meteorol. 140, 6 22. https://doi.org/10.1016/j.agrformet.2006.03.018.
Ikawa, H., Nakai, T., Busey, R.C., Kim, Y., Kobayashi, H., Nagai, S., Ueyama, M., Saito, K., Nagano, H., Suzuki, R., Hinzman, L., 2015. Understory CO_2, sensible heat, and latent heat fluxes in a black spruce forest in interior Alaska. Agric. For. Meteorol. 214 215, 80 90. https://doi.org/10.1016/j.agrformet.2015.08.247.
Iwahana G., Kobayashi H., Ikawa H., Suzuki R. (2019), AmeriFlux BASE US-Prr poker flat research range Black Spruce Forest, Ver. 3-5, AmeriFlux AMP, (Dataset). 10.17190/AMF/1246153.
Iwata, H., Ueyama, M., Iwama, C., Harazono, Y., 2013. Variations in fraction of absorbed photosynthetically active radiation and comparisons with MODIS data in burned black spruce forests of interior Alaska. Polar Sci. 7, 113 124. https://doi.org/10.1016/j.polar.2013.03.004.
Jonsson, P., Eklundh, L., 2004. TIMESAT - a program for analyzing time-series of satellite sensor data. Comput. Geosci. 30, 833 845. https://doi.org/10.1016/j.cageo.2004.05.006.
Jin, H., Eklundh, L., 2014. A physically based vegetation index for improved monitoring of plant phenology. Remote Sens. Environ. 152, 512 525. https://doi.org/10.1016/j.rse.2014.07.010.
Jin, H., Jonsson, A.M., Bolmgren, K., Langvall, O., Eklundh, L., 2017. Disentangling remotely-sensed plant phenology and snow seasonality at northern Europe using MODIS and the plant phenology index. Remote Sens. Environ. 198, 203 212. https://doi.org/10.1016/j.rse.2017.06.015.
Kelly, A.E., Goulden, M.L., 2016. A montane Mediterranean climate supports year-round photosynthesis and high forest biomass. Tree Physiol. 36, 459 468. https://doi.org/10.1093/treephys/tpv131.
Kirilenko, A.P., Sedjo, R.A., 2007. Climate change impacts on forestry. Proc. Natl. Acad. Sci. U. S. A. 104, 19697 19702. https://doi.org/10.1073/pnas.0701424104.
Kolb, T., Dore, S., Montes-Helu, M., 2013. Extreme late-summer drought causes neutral annual carbon balance in southwestern ponderosa pine forests and grasslands. Environ. Res. Lett. 8 https://doi.org/10.1088/1748-9326/8/1/015015.
Kurz, W.A., Shaw, C.H., Boisvenue, C., Stinson, G., Metsaranta, J., Leckie, D., Dyk, A., Smyth, C., Neilson, E.T., 2013. Carbon in Canada s boreal forest - a synthesis. Environ. Rev. 21, 260 292.
Lasslop, G., Reichstein, M., Papale, D., Richardson, A., Arneth, A., Barr, A., Stoy, P., Wohlfahrt, G., 2010. Separation of net ecosystem exchange into assimilation and respiration using a light response curve approach: critical issues and global evaluation. Glob. Change Biol. 16, 187 208. https://doi.org/10.1111/j.1365-2486.2009.02041.x.
Law B. (2018), AmeriFlux BASE US-Me3 Metolius-second young aged pine, Ver. 4-5, AmeriFlux AMP, (Dataset). 10.17190/AMF/1246077.
Law B. (2021), AmeriFlux BASE US-Me5 Metolius-first young aged pine, Ver. 3-5, AmeriFlux AMP, (Dataset). 10.17190/AMF/1246079.
Law B. (2021), AmeriFlux BASE US-Me6 Metolius Young Pine Burn, Ver. 15-5, AmeriFlux AMP, (Dataset). 10.17190/AMF/1246128.
Law B. (2022), AmeriFlux BASE US-Me2 Metolius mature ponderosa pine, Ver. 18-5, AmeriFlux AMP, (Dataset). 10.17190/AMF/1246076.
Litvak M. (2022), AmeriFlux BASE US-Vcm Valles Caldera Mixed Conifer, Ver. 22-5, AmeriFlux AMP, (Dataset). 10.17190/AMF/1246121.
Litvak M. (2022), AmeriFlux BASE US-Vcp Valles Caldera Ponderosa Pine, Ver. 19-5, AmeriFlux AMP, (Dataset). 10.17190/AMF/1246122.
Lv, Z., Pomeroy, J.W., 2019. Detecting intercepted snow on mountain needleleaf forest canopies using satellite remote sensing. Remote Sens. Environ. 231, 111222 https://doi.org/10.1016/j.rse.2019.111222.
Lyapustin, A.I., Wang, Y., Laszlo, I., Hilker, T., G.Hall, F., Sellers, P.J., Tucker, C.J., Korkin, S.V., 2012. Multi-angle implementation of atmospheric correction for MODIS (MAIAC): 3. atmospheric correction. Remote Sens. Environ. 127, 385 393. https://doi.org/10.1016/j.rse.2012.09.002.
Lyapustin, A., Wang, Y., Korkin, S., Huang, D., 2018. MODIS collection 6 MAIAC algorithm. Atmos. Meas. Tech. 11, 5741 5765. https://doi.org/10.5194/amt-11-5741-2018.
Magney, T.S., Bowling, D.R., Logan, B.A., Grossmann, K., Stutz, J., Blanken, P.D., Burns, S.P., Cheng, R., Garcia, M.A., Köhler, P., Lopez, S., Parazoo, N.C., Raczka, B., Schimel, D., Frankenberg, C., 2019. Mechanistic evidence for tracking the seasonality of photosynthesis with solar-induced fluorescence. Proc. Natl. Acad. Sci., 201900278 https://doi.org/10.1073/pnas.1900278116.
Margolis H.A. (2016), AmeriFlux BASE CA-Qcu Quebec - Eastern Boreal, Black Spruce/Jack Pine Cutover, Ver. 1-1, AmeriFlux AMP, (Dataset). 10.17190/AMF/1246828.
Margolis H.A. (2019), AmeriFlux BASE CA-Qfo Quebec - Eastern Boreal, Mature Black Spruce, Ver. 2-5, AmeriFlux AMP, (Dataset). 10.17190/AMF/1246829.
McCollum, C., Ibanez, I., 2020. Soil moisture gradients and climate change: predicting growth of a critical boreal tree species. Can. J. For. Res. 50, 1074 1080. https://doi.org/10.1139/cjfr-2019-0397.
McDowell, N.G., Williams, A.P., Xu, C., Pockman, W.T., Dickman, L.T., Sevanto, S., Pangle, R., Limousin, J., Plaut, J., Mackay, D.S., Ogee, J., Domec, J.C., Allen, C.D., Fisher, R.A., Jiang, X., Muss, J.D., Breshears, D.D., Rauscher, S.A., Koven, C., 2016. Multi-scale predictions of massive conifer mortality due to chronic temperature rise. Nat. Clim. Change 6, 295 300. https://doi.org/10.1038/nclimate2873.
McGill, R., Tukey, J.W., Larsen, W.A., 1978. Variations of box plots. Am. Stat. 32, 12 16.
McMahon, G., Gregonis, S.M., Waltman, S.W., Omernik, J.M., Thorson, T.D., Freeouf, J. A., Rorick, A.H., Keys, J.E., 2001. Developing a spatial framework of common ecological regions for the conterminous United States. Environ. Manag. 28, 293 316. https://doi.org/10.1007/s0026702429.
Meyers T. (2016), AmeriFlux BASE US-Blk Black Hills, Ver. 2-1, AmeriFlux AMP, (Dataset). 10.17190/AMF/1246031.
Middleton, E.M., Huemmrich, K.F., Landis, D.R., Black, T.A., Barr, A.G., McCaughey, J. H., 2016. Photosynthetic efficiency of northern forest ecosystems using a MODIS-derived photochemical reflectance index (PRI). Remote Sens. Environ. 187, 345 366. https://doi.org/10.1016/j.rse.2016.10.021.
Myers-Smith, I.H., Kerby, J.T., Phoenix, G.K., Bjerke, J.W., Epstein, H.E., Assmann, J.J., John, C., Andreu-Hayles, L., Angers-Blondin, S., Beck, P.S.A., Berner, L.T., Bhatt, U. S., Bjorkman, A.D., Blok, D., Bryn, A., Christiansen, C.T., Cornelissen, J.H.C., Cunliffe, A.M., Elmendorf, S.C., Forbes, B.C., Goetz, S.J., Hollister, R.D., de Jong, R., Loranty, M.M., Macias-Fauria, M., Maseyk, K., Normand, S., Olofsson, J., Parker, T. C., Parmentier, F.J.W., Post, E., Schaepman-Strub, G., Stordal, F., Sullivan, P.F., Thomas, H.J.D., T mmervik, H., Treharne, R., Tweedie, C.E., Walker, D.A., Wilmking, M., Wipf, S., 2020. Complexity revealed in the greening of the Arctic. Nat. Clim. Change 10, 106 117. https://doi.org/10.1038/s41558-019-0688-1.
NEON (National Ecological Observatory Network) (2022), AmeriFlux BASE US-xDJ NEON Delta Junction (DEJU), Ver. 6-5, AmeriFlux AMP, (Dataset). 10.17190/AMF/1634884.
NEON (National Ecological Observatory Network) (2022), AmeriFlux BASE US-xWR NEON Wind River Experimental Forest (WREF), Ver. 6-5, AmeriFlux AMP, (Dataset). 10.17190/AMF/161774.
NEON (National Ecological Observatory Network) (2022), AmeriFlux BASE US-xAB NEON Abby Road (ABBY), Ver. 6-5, AmeriFlux AMP, (Dataset). 10.17190/AMF/1617726.
NEON (National Ecological Observatory Network) (2022), AmeriFlux BASE US-xTA NEON Talladega National Forest (TALL), Ver. 5-5, AmeriFlux AMP, (Dataset). 10.17190/AMF/1671902.
NEON (National Ecological Observatory Network) (2022), AmeriFlux BASE US-xJE NEON Jones Ecological Research Center (JERC), Ver. 6-5, AmeriFlux AMP, (Dataset). 10.17190/AMF/1617730.
NEON (National Ecological Observatory Network) (2022), AmeriFlux BASE US-xSB NEON Ordway-Swisher Biological Station (OSBS), Ver. 5-5, AmeriFlux AMP, (Dataset). 10.17190/AMF/1671899.
Noormets A., Sun G., Gavazzi M., Domec J., McNulty S., Miao G., Aguilos M., Mitra B., Minick K., King J., Yang L., Prajapati P. (2022), AmeriFlux BASE US-NC2 NC_Loblolly Plantation, Ver. 10-5, AmeriFlux AMP, (Dataset). 10.17190/AMF/1246083.
Omernik, J.M., Griffith, G.E., 2014. Ecoregions of the conterminous United States: evolution of a hierarchical spatial framework. Environ. Manag. 54, 1249 1266. https://doi.org/10.1007/s00267-014-0364-1.
Pastorello, G., Trotta, C., Canfora, E., Chu, H., Christianson, D., Cheah, Y.W., Poindexter, C., Chen, J., Elbashandy, A., Humphrey, M., Isaac, P., Polidori, D., Ribeca, A., van Ingen, C., Zhang, L., Amiro, B., Ammann, C., Arain, M.A., Ardo, J., Arkebauer, T., Arndt, S.K., Arriga, N., Aubinet, M., Aurela, M., Baldocchi, D., Barr, A., Beamesderfer, E., Marchesini, L.B., Bergeron, O., Beringer, J., Bernhofer, C., Berveiller, D., Billesbach, D., Black, T.A., Blanken, P.D., Bohrer, G., Boike, J., Bolstad, P.V., Bonal, D., Bonnefond, J.M., Bowling, D.R., Bracho, R., Brodeur, J., Brümmer, C., Buchmann, N., Burban, B., Burns, S.P., Buysse, P., Cale, P., Cavagna, M., Cellier, P., Chen, S., Chini, I., Christensen, T.R., Cleverly, J., Collalti, A., Consalvo, C., Cook, B.D., Cook, D., Coursolle, C., Cremonese, E., Curtis, P.S., D Andrea, E., da Rocha, H., Dai, X., Davis, K.J., De Cinti, B., de Grandcourt, A., De Ligne, A., De Oliveira, R.C., Delpierre, N., Desai, A.R., Di Bella, C. M., di Tommasi, P., Dolman, H., Domingo, F., Dong, G., Dore, S., Duce, P.,

Dufrene, E., Dunn, A., Dusek, J., Eamus, D., Eichelmann, U., ElKhidir, H.A.M., Eugster, W., Ewenz, C.M., Ewers, B., Famulari, D., Fares, S., Feigenwinter, I., Feitz, A., Fensholt, R., Filippa, G., Fischer, M., Frank, J., Galvagno, M., Gharun, M., Gianelle, D., Gielen, B., Gioli, B., Gitelson, A., Goded, I., Goeckede, M., Goldstein, A. H., Gough, C.M., Goulden, M.L., Graf, A., Griebel, A., Gruening, C., Grünwald, T., Hammerle, A., Han, S., Han, X., Hansen, B.U., Hanson, C., Hatakka, J., He, Y., Hehn, M., Heinesch, B., Hinko-Najera, N., Hortnagl, L., Hutley, L., Ibrom, A., Ikawa, H., Jackowicz-Korczynski, M., Janous, D., Jans, W., Jassal, R., Jiang, S., Kato, T., Khomik, M., Klatt, J., Knohl, A., Knox, S., Kobayashi, H., Koerber, G., Kolle, O., Kosugi, Y., Kotani, A., Kowalski, A., Kruijt, B., Kurbatova, J., Kutsch, W.L., Kwon, H., Launiainen, S., Laurila, T., Law, B., Leuning, R., Li, Yingnian, Liddell, M., Limousin, J.M., Lion, M., Liska, A.J., Lohila, A., Lopez-Ballesteros, A., Lopez-Blanco, E., Loubet, B., Loustau, D., Lucas-Moffat, A., Lüers, J., Ma, S., Macfarlane, C., Magliulo, V., Maier, R., Mammarella, I., Manca, G., Marcolla, B., Margolis, H.A., Marras, S., Massman, W., Mastepanov, M., Matamala, R., Matthes, J.H., Mazzenga, F., McCaughey, H., McHugh, I., McMillan, A.M.S., Merbold, L., Meyer, W., Meyers, T., Miller, S.D., Minerbi, S., Moderow, U., Monson, R.K., Montagnani, L., Moore, C.E., Moors, E., Moreaux, V., Moureaux, C., Munger, J.W., Nakai, T., Neirynck, J., Nesic, Z., Nicolini, G., Noormets, A., Northwood, M., Nosetto, M., Nouvellon, Y., Novick, K., Oechel, W., Olesen, J.E., Ourcival, J.M., Papuga, S.A., Parmentier, F.J., Paul-Limoges, E., Pavelka, M., Peichl, M., Pendall, E., Phillips, R.P., Pilegaard, K., Pirk, N., Posse, G., Powell, T., Prasse, H., Prober, S.M., Rambal, S., Rannik, Ü., Raz-Yaseef, N., Reed, D., de Dios, V.R., Restrepo-Coupe, N., Reverter, B.R., Roland, M., Sabbatini, S., Sachs, T., Saleska, S.R., Sanchez-Canete, E. P., Sanchez-Mejia, Z.M., Schmid, H.P., Schmidt, M., Schneider, K., Schrader, F., Schroder, I., Scott, R.L., Sedlak, P., Serrano-Ortíz, P., Shao, C., Shi, P., Shironya, I., Siebicke, L., Sigut, L., Silberstein, R., Sirca, C., Spano, D., Steinbrecher, R., Stevens, R.M., Sturtevant, C., Suyker, A., Tagesson, T., Takanashi, S., Tang, Y., Tapper, N., Thom, J., Tiedemann, F., Tomassucci, M., Tuovinen, J.P., Urbanski, S., Valentini, R., van der Molen, M., van Gorsel, E., van Huissteden, K., Varlagin, A., Verfaillie, J., Vesala, T., Vincke, C., Vitale, D., Vygodskaya, N., Walker, J.P., Walter-Shea, E., Wang, H., Weber, R., Westermann, S., Wille, C., Wofsy, S., Wohlfahrt, G., Wolf, S., Woodgate, W., Li, Yuelin, Zampedri, R., Zhang, J., Zhou, G., Zona, D., Agarwal, D., Biraud, S., Torn, M., Papale, D., 2020. The FLUXNET2015 dataset and the ONEFlux processing pipeline for eddy covariance data. Sci. Data 7, 225. https://doi.org/10.1038/s41597-020-0534-3.

Peng, Y., Nguy-Robertson, A., Arkebauer, T., Gitelson, A.A., 2017. Assessment of canopy chlorophyll content retrieval in maize and soybean: implications of hysteresis on the development of generic algorithms. Remote Sens. 9 https://doi.org/10.3390/rs9030226.

Pierrat, Z., Magney, T., Parazoo, N.C., Grossmann, K., Bowling, D.R., Seibt, U., Johnson, B., Helgason, W., Barr, A., Bortnik, J., Norton, A., Maguire, A., Frankenberg, C., Stutz, J., 2022. Diurnal and seasonal dynamics of solar-induced chlorophyll fluorescence, vegetation indices, and gross primary productivity in the Boreal Forest. J. Geophys. Res. Biogeosciences 127, e2021JG006588. https://doi.org/10.1029/2021JG006588.

Rahman, A.F., Cordova, V.D., Gamon, J.A., Schmid, H.P., Sims, D.A., 2004. Potential of MODIS ocean bands for estimating CO_2 flux from terrestrial vegetation: a novel approach. Geophys. Res. Lett. 31, 3 6. https://doi.org/10.1029/2004GL019778.

Randerson J. (2016), AmeriFlux BASE US-Bn1 Bonanza Creek, 1920 Burn site near Delta Junction, Ver. 1-1, AmeriFlux AMP, (Dataset). 10.17190/AMF/1246033.

Reichstein, M., Falge, E., Baldocchi, D., Papale, D., Aubinet, M., Berbigier, P., Bernhofer, C., Buchmann, N., Gilmanov, T., Granier, A., Grünwald, T., Havrankova, K., Ilvesniemi, H., Janous, D., Knohl, A., Laurila, T., Lohila, A., Loustau, D., Matteucci, G., Meyers, T., Miglietta, F., Ourcival, J.M., Pumpanen, J., Rambal, S., Rotenberg, E., Sanz, M., Tenhunen, J., Seufert, G., Vaccari, F., Vesala, T., Yakir, D., Valentini, R., 2005. On the separation of net ecosystem exchange into assimilation and ecosystem respiration: review and improved algorithm. Glob. Change Biol. 11, 1424 1439. https://doi.org/10.1111/j.1365-2486.2005.001002.x.

Riggs G.A., Hall D., Roman M.O., 2016. MODIS snow products collection 6 user guide.

Running, S.W., Nemani, R.R., Heinsch, F.A., Zhao, M., Reeves, M., Hashimoto, H., 2004. A continuous satellite-derived measure of global terrestrial primary production. Bioscience 54, 547 560. https://doi.org/10.1641/0006-3568(2004)054[0547:ACSMOG]2.0.CO;2.

Ryu, Y., Berry, J.A., Baldocchi, D.D., 2019. What is global photosynthesis? History, uncertainties and opportunities. Remote Sens. Environ. 223, 95 114. https://doi.org/10.1016/j.rse.2019.01.016.

Sarmah, S., Singha, M., Wang, J., Dong, J., Deb Burman, P.K., Goswami, S., Ge, Y., Ilyas, S., Niu, S., 2021. Mismatches between vegetation greening and primary productivity trends in South Asia a satellite evidence. Int. J. Appl. Earth Obs. Geoinf. 104 (May), 102561 https://doi.org/10.1016/j.jag.2021.102561.

Sevanto, S., Suni, T., Pumpanen, J., Gronholm, T., Kolari, P., Nikinmaa, E., Hari, P., Vesala, T., 2006. Wintertime photosynthesis and water uptake in a boreal forest. Tree Physiol. 26, 749 757. https://doi.org/10.1093/treephys/26.6.749.

Seyednasrollah, B., Young, A.M., Hufkens, K., Milliman, T., Friedl, M.A., Frolking, S., Richardson, A.D., 2019. Tracking vegetation phenology across diverse biomes using version 2.0 of the PhenoCam dataset. Sci. Data 6, 1 11. https://doi.org/10.1038/s41597-019-0229-9.

Seyednasrollah, B., Bowling, D.R., Cheng, R., Logan, B.A., Magney, T.S., Frankenberg, C., Yang, J.C., Young, A.M., Hufkens, K., Arain, M.A., Black, T.A., Blanken, P.D., Bracho, R., Jassal, R., Hollinger, D.Y., Law, B.E., Nesic, Z., Richardson, A.D., 2021. Seasonal variation in the canopy color of temperate evergreen conifer forests. New Phytol. 229, 2586 2600. https://doi.org/10.1111/nph.17046.

Shen, M., Zhang, G., Cong, N., Wang, S., Kong, W., Piao, S., 2014. Increasing altitudinal gradient of spring vegetation phenology during the last decade on the Qinghai-Tibetan Plateau. Agric. For. Meteorol. 189 190 (71 80) https://doi.org/10.1016/j.agrformet.2014.01.003.

Sims, D.A., Luo, H., Hastings, S., Oechel, W.C., Rahman, A.F., Gamon, J.A., 2006. Parallel adjustments in vegetation greenness and ecosystem CO_2 exchange in response to drought in a Southern California chaparral ecosystem. Remote Sens. Environ. 103, 289 303. https://doi.org/10.1016/j.rse.2005.01.020.

Snoek J., Larochelle H., Adams R.P., 2012. Practical Bayesian optimization of machine learning algorithms, in: practical Bayesian optimization of machine learning algorithms. pp. 2960 2968. 10.1163/15685292-12341254.

Springer, K.R., Wang, R., Gamon, J.A., 2017. Parallel seasonal patterns of photosynthesis, fluorescence, and reflectance indices in boreal trees. Remote Sens. 9, 1 18. https://doi.org/10.3390/rs9070691.

Stefano, P., Angelo, P., Simone, P., Filomena, R., Federico, S., Tiziana, S., Umberto, A., Vincenzo, C., Acito, N., Marco, D., Stefania, M., Giovanni, C., Raffaele, C., Roberto, D.B., Giovanni, L., Cristina, A., 2013. The PRISMA hyperspectral mission: science activities and opportunities for agriculture and land monitoring. In: Proceedings of the International Geoscience and Remote Sensing Symposium (IGARSS). Melbourne, Australia, pp. 4558 4561. https://doi.org/10.1109/IGARSS.2013.6723850.

Stralberg, D., Arseneault, D., Baltzer, J.L., Barber, Q.E., Bayne, E.M., Boulanger, Y., Brown, C.D., Cooke, H.A., Devito, K., Edwards, J., Estevo, C.A., Flynn, N., Frelich, L. E., Hogg, E.H., Johnston, M., Logan, T., Matsuoka, S.M., Moore, P., Morelli, T.L., Whitman, E., 2020. Climate-change refugia in boreal North America: what, where, and for how long? Front. Ecol. Environ. 18 (5), 261 270. https://doi.org/10.1002/fee.2188.

Suarez, L., Zarco-Tejada, P.J., Sepulcre-Canto, G., Perez-Priego, O., Miller, J.R., Jimenez-Munoz, J.C., Sobrino, J., 2008. Assessing canopy PRI for water stress detection with diurnal airborne imagery. Remote Sens. Environ. 112 (2), 560 575. https://doi.org/10.1016/j.rse.2007.05.009.

Suarez, L., Zarco-Tejada, P.J., Gonzalez-Dugo, V., Berni, J., Sagardoy, R., Morales, F., Fereres, E., 2010. Detecting water stress effects on fruit quality in orchards with time-series PRI airborne imagery. Remote Sens. Environ. 114 (2), 286 298. https://doi.org/10.1016/j.rse.2009.09.006.

Thompson, J.R., Carpenter, D.N., Cogbill, C.V., Foster, D.R., 2013. Four centuries of change in Northeastern United States Forests. PLoS One 8. https://doi.org/10.1371/journal.pone.0072540.

Turcotte, A., Morin, H., Krause, C., Deslauriers, A., Thibeault-Martel, M., 2009. The timing of spring rehydration and its relation with the onset of wood formation in black spruce. Agric. For. Meteorol. 149, 1403 1409. https://doi.org/10.1016/j.agrformet.2009.03.010.

Ueyama M., Iwata H., Harazono Y. (2023), AmeriFlux BASE US-Uaf University of Alaska, Fairbanks, Ver. 11-5, AmeriFlux AMP, (Dataset). 10.17190/AMF/1480322.

Verhoeven, A., 2014. Sustained energy dissipation in winter evergreens. New Phytol. 201, 57 65. https://doi.org/10.1111/nph.12466.

Walter-McNeill, A., Garcia, M.A., Logan, B.A., Bombard, D.M., Reblin, J.S., Lopez, S., Southwick, C.D., Sparrow, E.L., Bowling, D.R., 2021. Wide variation of winter-induced sustained thermal energy dissipation in conifers: a common-garden study. Oecologia 197, 589 598. https://doi.org/10.1007/s00442-021-05038-y.

Wang, X., Wang, J., Che, T., Huang, X., Hao, X., Li, H., 2018. Snow cover mapping for complex mountainous forested environments based on a multi-index technique. IEEE J. Sel. Top. Appl. Earth Obs. Remote Sens. 11, 1433 1441. https://doi.org/10.1109/JSTARS.2018.2810094.

Wang, R., Gamon, J.A., Emmerton, C.A., Springer, K.R., Yu, R., Hmimina, G., 2020. Detecting intra- and inter-annual variability in gross primary productivity of a North American grassland using MODIS MAIAC data. Agric. For. Meteorol. 281, 107859 https://doi.org/10.1016/j.agrformet.2019.107859.

Wang, R., Springer, K.R., Gamon, J.A., 2023. Confounding effects of snow cover on remotely sensed vegetation indices of evergreen and deciduous trees: an experimental study. Global Change Biology. In press.

Wells, J.V., Dawson, N., Culver, N., Reid, F.A., Morgan Siegers, S., 2020. The state of conservation in North America s Boreal Forest: issues and opportunities. Front. For. Glob. Change 3 (July), 1 18. https://doi.org/10.3389/ffgc.2020.00090.

Wharton S. (2016), AmeriFlux BASE US-Wrc Wind River Crane Site, Ver. 8-1, AmeriFlux AMP, (Dataset). 10.17190/AMF/1246114.

White, J.C., Wulder, M.A., Hermosilla, T., Coops, N.C., Hobart, G.W., 2017. A nationwide annual characterization of 25 years of forest disturbance and recovery for Canada using Landsat time series. Remote Sens. Environ. 194, 303 321. https://doi.org/10.1016/j.rse.2017.03.035.

Williams, A.P., Allen, C.D., Macalady, A.K., Griffin, D., Woodhouse, C.A., Meko, D.M., Swetnam, T.W., Rauscher, S.A., Seager, R., Grissino-Mayer, H.D., Dean, J.S., Cook, E. R., Gangodagamage, C., Cai, M., Mcdowell, N.G., 2013. Temperature as a potent driver of regional forest drought stress and tree mortality. Nat. Clim. Change 3, 292 297. https://doi.org/10.1038/nclimate1693.

Wong, C.Y.S., Gamon, J.A., 2015. The photochemical reflectance index provides an optical indicator of spring photosynthetic activation in evergreen conifers. New Phytol. 206, 196 208. https://doi.org/10.1111/nph.13251.

Wong, C.Y.S., D Odorico, P., Arain, M.A., Ensminger, I., 2020. Tracking the phenology of photosynthesis using carotenoid-sensitive and near-infrared reflectance vegetation indices in a temperate evergreen and mixed deciduous forest. New Phytol. 226, 1682 1695. https://doi.org/10.1111/nph.16479.

Wong, C.Y.S., Mercado, L.M., Arain, M.A., Ensminger, I., 2022. Remotely sensed carotenoid dynamics improve modelling photosynthetic phenology in conifer and deciduous forests. Agric. For. Meteorol. 321, 108977 https://doi.org/10.1016/j.agrformet.2022.108977.

Wutzler, T., Lucas-Moffat, A., Migliavacca, M., Knauer, J., Sickel, K., Sigut, L., Menzer, O., Reichstein, M., 2018. Basic and extensible post-processing of eddy

covariance flux data with REddyProc. Biogeosciences 15, 5015 5030. https://doi.org/10.5194/bg-15-5015-2018.

Xu, B., Arain, M.A., Black, T.A., Law, B.E., Pastorello, G.Z., Chu, H., 2020. Seasonal variability of forest sensitivity to heat and drought stresses: a synthesis based on carbon fluxes from North American forest ecosystems. Glob. Change Biol. 26 (2), 901 918. https://doi.org/10.1111/gcb.14843.

Yamazaki, D., Ikeshima, D., Tawatari, R., Yamaguchi, T., O Loughlin, F., Neal, J.C., Sampson, C.C., Kanae, S., Bates, P.D., 2017. A high-accuracy map of global terrain elevations. Geophys. Res. Lett. 44, 5844 5853. https://doi.org/10.1002/2017GL072874.

Yan, K., Park, T., Yan, G., Liu, Z., Yang, B., Chen, C., Nemani, R.R., Knyazikhin, Y., Myneni, R.B., 2016. Evaluation of MODIS LAI/FPAR product collection 6. part 2: validation and intercomparison. Remote Sens. 8 https://doi.org/10.3390/rs8060460.

Yang, J.C., Magney, T.S., Albert, L.P., Richardson, A.D., Frankenberg, C., Stutz, J., Grossmann, K., Burns, S.P., Seyednasrollah, B., Blanken, P.D., Bowling, D.R., 2022. Gross primary production (GPP) and red solar induced fluorescence (SIF) respond differently to light and seasonal environmental conditions in a subalpine conifer forest. Agric. For. Meteorol. 317, 108904 https://doi.org/10.1016/j.agrformet.2022.108904.

Zarco-Tejada, P.J., Gonzalez-Dugo, V., Berni, J.A.J., 2012. Fluorescence, temperature and narrow-band indices acquired from a UAV platform for water stress detection using a micro-hyperspectral imager and a thermal camera. Remote Sens. Environ. 117, 322 337. https://doi.org/10.1016/j.rse.2011.10.007.

Zeng, Y., Hao, D., Huete, A., Dechant, B., Berry, J., Chen, J.M., Joiner, J., Frankenberg, C., Bond-Lamberty, B., Ryu, Y., Xiao, J., Asrar, G.R., Chen, M., 2022. Optical vegetation indices for monitoring terrestrial ecosystems globally. Nat. Rev. Earth Environ. 3, 477 493. https://doi.org/10.1038/s43017-022-00298-5.

Zhang, Y., Xiao, X., Zhou, S., Ciais, P., McCarthy, H., Luo, Y., 2016. Canopy and physiological controls of GPP during drought and heat wave. Geophys Res. Lett. 43 (7), 3325 3333. https://doi.org/10.1002/2016GL068501.

Zhang, Y., Piao, S., Sun, Y., Rogers, B.M., Li, X., Lian, X., Liu, Z., Chen, A., Penuelas, J., 2022. Future reversal of warming-enhanced vegetation productivity in the Northern Hemisphere. Nat. Clim. Change 12 (6), 581 586. https://doi.org/10.1038/s41558-022-01374-w.